

Surface response of exchange- and dipolar-coupled ferromagnets: Application to light scattering from magnetic surfaces

R. E. Camley and D. L. Mills

Department of Physics, University of California, Irvine, California 92717

(Received 15 May 1978)

We present the theory of the surface response of a semi-infinite ferromagnet in the presence of both exchange and dipolar coupling, within a continuum theory. The results are applied to a detailed study of the spectral density of surface spin fluctuations. From this we analyze the influence of exchange coupling and surface spin pinning on the frequency, linewidth, and line shape of the Damon-Eshbach surface spin wave, for a number of propagation angles, and for wavelengths sufficiently short that the exchange contribution to the energy of the wave is comparable to the Zeeman and dipolar energies. We also develop the theory of Brillouin scattering from spin waves near magnetic surfaces, and calculate the spectrum of scattered light for experimentally interesting geometries, with recent light scattering studies of ferromagnetic surfaces in mind.

I. INTRODUCTORY REMARKS

The nature of magnetism at the surface of crystals has been the topic of numerous theoretical papers during the past few years. For a semi-infinite Heisenberg ferromagnet¹ or antiferromagnet,² the mean-spin deviation near the surface can differ substantially from the bulk. In addition, magnetic instabilities can occur at the surface under a range of conditions^{3,4} to influence a variety of measurements.⁵

At this time, no systematic body of data exists which can be brought to bear on these issues, although a number of measurements⁶⁻⁹ suggest anomalous behavior at surfaces consistent with the presence of magnetic instabilities,⁵ or spin canting¹⁰ induced by the combined action of an external Zeeman field and surface anisotropy. We believe new experimental probes, such as the study of Rayleigh-wave propagation on magnetic crystals,¹¹ may prove a useful supplement to the magnetic-resonance^{6,7} and light-scattering^{8,9} studies which have provided information on magnetic surfaces.

The experimental methods just cited, while they can probe features of the magnetic response sensitive to the magnetic configuration of the outermost atomic layers, have the common property that they excite spin motions that vary slowly in space on the scale of the lattice constant. In the microwave-resonance studies, it is the film thickness that sets the length scale.¹² In the light-scattering experiment, the wavelength of the light in vacuum and the skin depth both enter as we shall see here, and in Rayleigh-wave-propagation studies the wavelength of the Rayleigh wave sets the length scale.

When spin waves in ferromagnets with wavelength long compared to the lattice constant are

excited, then the magnetic dipole moments of the spins set up macroscopic magnetic fields that can influence the excitation energies of the spin waves importantly. The analysis of the spin-wave spectrum in the bulk in the presence of both exchange and dipolar interactions between the spins is a textbook topic.¹³ Rather little attention has been devoted to this topic, for spins near the surface of a semi-infinite ferromagnet with both exchange and magnetic dipole coupling present.¹⁴ The purpose of this paper is to provide a description of the surface response in this regime of sufficient generality for use in a variety of analyses, extract information from it about the nature of surface spin waves with both dipolar and exchange coupling present, and then apply the formalism to an analysis of light scattering from spin waves at the surface of a ferromagnet. This application is motivated by the very beautiful studies of spin waves at ferromagnetic surfaces reported recently by Metawe and Grünberg,⁸ and by Wettling and Sandercock.⁹ We have here the first studies of magnetic excitations near a surface in a system that is an excellent approximation to a semi-infinite geometry.

Before we proceed with the technical discussion, a few introductory remarks may be a useful means of orienting the reader.

At long wavelengths, exchange interactions play a small role in spin-wave theory, and the excitation energy of spin waves receives its dominant contribution from the external Zeeman field, and the demagnetizing fields set up by the spin motion. The frequency $\Omega_B(\vec{k})$ of a bulk spin wave then depends only on the angle between its wave vector \vec{k} , and the direction \hat{z} of the magnetization M_s . The frequency is independent of the magnitude of \vec{k} , when its direction is fixed. The minimum bulk-spin-wave frequency Ω_M occurs for propagation

parallel to \hat{z} , and the maximum Ω_M for propagation in the plane perpendicular to \hat{z} . We have $\Omega_m = \gamma H$ and $\Omega_M = \gamma(HB)^{1/2}$, where H is the externally applied Zeeman field, $B = H + 4\pi M_s$, and γ is the gyro-magnetic ratio. The frequency regime $\Omega_m \leq \Omega \leq \Omega_M$ is referred to as the bulk-spin-wave manifold.

With surface present, exchange still ignored, and magnetization direction \hat{z} parallel to the surface, one finds a surface spin wave with frequency $\Omega_s(\vec{k}_{\parallel})$ that also depends on the angle between the wave vector \vec{k}_{\parallel} and \hat{z} ; of course, \vec{k}_{\parallel} is parallel to the surface. This wave, called the Damon-Eshbach (DE) mode in much of the literature, has two unusual properties. Firstly, its frequency lies *above* the bulk-spin-wave manifold. Depending on the direction of propagation, it lies between Ω_M and $\Omega_{DE} = \frac{1}{2}\gamma(H+B)$, a frequency larger than Ω_M . This property contrasts sharply with other well-known examples of surface waves. Secondly, the DE surface spin wave exists only if \vec{k}_{\parallel} is directed into a restricted range of angles. Let \hat{x} and \hat{z} be parallel to the surface, \hat{y} normal to the surface, with the crystal in the half space $y > 0$. Then let θ be the angle between \vec{k}_{\parallel} and \hat{x} . This geometry is illustrated in Fig. 1. One finds the DE wave propagates only in the angular range $\theta = \pi \pm \psi_c$, where the critical angle ψ_c is given by $\cos(\psi_c) = (H/B)^{1/2}$. The dispersion relation is highly nonreciprocal, i.e., $\Omega_s(\vec{k}_{\parallel}) \neq \Omega_s(-\vec{k}_{\parallel})$. Indeed, no surface wave propagation is possible for waves moving from left to right (i.e., from $-x$ to $+x$) on the surface. In the light-scattering experiments mentioned above,^{8,9} one finds a most elegant demonstration of this nonreciprocity. For *fixed scattering angle*, if the DE wave appears in the Stokes spectrum, it fails to appear on the anti-Stokes side and conversely.

The above discussion neglects the role of exchange. With exchange added, the frequency $\Omega_B(\vec{k})$ of a bulk spin wave is upshifted by terms in Dk^2 , with D the exchange stiffness constant. For $Dk^2 \gg \gamma H$ or γB , $\Omega_B(\vec{k}) \cong Dk^2$. In the presence of exchange, there are thus bulk spin waves degenerate with the DE wave, by virtue of the exchange. As first pointed out by Wolfram and de Wames,¹⁴ the DE wave then becomes a "leaky surface wave."

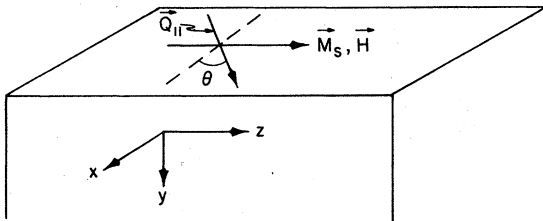


FIG. 1. Geometry and coordinate axes that form the basis of the discussion in Secs. I and II.

If a surface disturbance in the form of a DE wave is set up at time $t=0$, then the energy density stored near the surface decays to zero after a characteristic time. The surface wave decays by radiating its stored energy in the form of bulk spin waves.

Wolfram and de Wames¹⁴ calculate the radiative lifetime and the frequency shift from exchange for the DE wave by a method that presumes the exchange is small. In essence, they proceed by setting up a surface disturbance with (real) wave vector \vec{k}_{\parallel} , then following its subsequent time dependence. This is done only for one angle of propagation, $\theta = \pi$, in our earlier notation.

We proceed quite differently here, since the approach used in Ref. 14 seems somewhat artificial to us. No experimental probe directly examines the time profile of a surface disturbance with real wave vector, for example.

By a method described below, we prefer to analyze the frequency spectrum of thermal spin fluctuations near the surface. By the fluctuation-dissipation theorem, this information also enables us to construct the response of the surface region to specific external probes. The light-scattering experiments^{8,9} provide examples of a powerful method of probing these fluctuations. Our analysis of the spin-fluctuation spectrum leads us to a spectral density function $A(\vec{Q}_{\parallel}, \Omega; y)$ with the following physical interpretation. If one samples a slab of material parallel to the surface, a distance y from it and with thickness dy , then $A(\vec{Q}_{\parallel}, \Omega; y)dy$ is a measure of the amplitude of the thermal spin fluctuations in the slab with frequency Ω and wave vector \vec{Q}_{\parallel} . The DE wave shows as a prominent δ -function-like peak in the surface response function $A(\vec{Q}_{\parallel}, \Omega; y=0)$ for \vec{Q}_{\parallel} small enough that exchange effects are small. As the wavelength shortens, the importance of exchange becomes evident by a broadening of the surface mode peak and a shift to higher frequency. From the position and width of the surface-wave feature, we have an operational definition of the frequency, inverse lifetime, and mean free path of the mode. By this means, we have carried out an extensive study of the influence of exchange and surface spin pinning on the DE mode, for a wide range of propagation angles and wave vectors. We do not need to assume the exchange is a small perturbation, and we are able to examine the nature of the spectral density even when DQ_{\parallel}^2 is so large that the surface mode is nearly critically damped by radiative processes.

As the reader shall appreciate, we find that the influence of exchange on the spectral density cannot be described by simply assigning a lifetime and frequency shift to the DE wave. As DQ_{\parallel}^2 , the

measure of the importance of exchange, increases the surface-spin-wave feature in $A(\vec{Q}_\parallel, \Omega; y=0)$ not only broadens but becomes distinctly asymmetric, to develop a pronounced tail at high frequency. As we move into the crystal and examine $A(\vec{Q}_\parallel, \Omega; y)$ for $y \neq 0$, the spectral density acquires rich structure with origin in interference beats between the several waves that are superimposed to form the DE leaky-surface wave in the presence of exchange. Finally, our method produces in addition to the shape of the surface mode structure in $A(\vec{Q}_\parallel, \Omega; y)$, its integrated strength as well. The variation of the integrated strength with angle and DQ_\parallel^2 provides a measure of one's ability to excite the wave with an external probe.

The method here is very similar in spirit to recent Green's-function descriptions of light scattering from polaritons in confined geometries.¹⁵ This method, and the closely related response-function description developed by Nkoma and Loudon,¹⁶ can be applied to a wide variety of problems where one wishes to analyze the long-wavelength response of a finite system. We call attention to recent work with these methods on Brillouin scattering by acoustical phonons near surfaces,¹⁷ an analysis of the scattering of Rayleigh acoustical surface waves by roughness on the surface,¹⁸ and the mean-square atomic displacement in elastic continua near surfaces.¹⁹

The outline of this paper is as follows. Section II develops the general theory and Sec. III summarizes our study of the DE feature in the spectral density of the surface spins. Then in Sec. IV we address the question of light scattering from a ferromagnetic surface and in Sec. V we compare our results to the recent experiments.

II. THEORY OF THE SURFACE RESPONSE OF A SEMI-INFINITE FERROMAGNET

We consider a semi-infinite ferromagnet with Zeeman field \vec{H} applied parallel to the surface. Thus, the magnetization \vec{M}_s lies parallel to the surface. The coordinate axis \hat{z} is aligned along the magnetization, \hat{y} is normal to the surface, and consequently \hat{x} lies parallel to the surface.

Suppose we probe the response of the system by subjecting it to a time-dependent magnetic field $\vec{h}(\vec{x}, t)$ with j th Cartesian component $h_j(\vec{x}, t)$. If $S_i(\vec{x}, t)$ is the i th component of spin density, then the expectation value $\langle S_i(\vec{x}, t) \rangle$ in the presence of $\vec{h}(\vec{x}, t)$ may be found once the susceptibility response functions $\chi_{ij}(\vec{x}, \vec{x}'; t-t')$ are known.²⁰ We have (with $\hbar=1$)

$$\langle S_i(\vec{x}, t) \rangle = g\mu_B \int_{-\infty}^{\infty} dt' \int d^3x' \sum_j \chi_{ij}(\vec{x}, \vec{x}'; t-t') h_j(\vec{x}', t'), \quad (2.1)$$

where μ_B is the Bohr magneton, g is the Landé g factor, and the integration ranges over the volume of the semi-infinite sample. The response function $\chi_{ij}(\vec{x}, \vec{x}'; t-t')$ is related to the spin densities through the Kubo formula

$$\chi_{ij}(\vec{x}, \vec{x}'; t-t') = +i\theta(t-t') \langle [S_i(\vec{x}, t), S_j(\vec{x}', t')] \rangle_0, \quad (2.2)$$

where $S_i(\vec{x}, t)$ is the time-dependent spin-density operator in the Heisenberg representation, $[A, B]$ is the commutator of the two operators A and B , and $\langle A \rangle_0$ is the expectation value of A for a statistical ensemble with $\vec{h}(\vec{r}, t) = 0$.

We shall wish to consider the spin correlation functions

$$S_{ij}(\vec{x}, \vec{x}'; t-t') = \langle S_i(\vec{x}, t) S_j(\vec{x}', t') \rangle_0 \quad (2.3)$$

in our study of spin fluctuations near the surface. We write

$$S_{ij}(\vec{x}, \vec{x}'; t-t') = \int_{-\infty}^{\infty} \frac{d\Omega}{2\pi} S_{ij}(\vec{x}, \vec{x}'; \Omega) e^{-i\Omega(t-t')} \quad (2.4)$$

with $\chi_{ij}(\vec{x}, \vec{x}'; \Omega)$ the Fourier transform of

$\chi_{ij}(\vec{x}, \vec{x}'; t-t')$ defined in a similar fashion, and $\chi_{ij}(\vec{x}, \vec{x}'; z)$ the analytic continuation of $\chi_{ij}(\vec{x}, \vec{x}'; \Omega)$ into the complex frequency plane from the near vicinity of the real axis.

By examining the structure of $S_{ij}(\vec{x}, \vec{x}'; \Omega)$ and $\chi_{ij}(\vec{x}, \vec{x}'; z)$ by writing their form out explicitly, one obtains a relation between the two; with $n(\Omega) = [\exp(\Omega/k_B T) - 1]^{-1}$ the Bose-Einstein function:

$$S_{ij}(\vec{x}, \vec{x}'; \Omega) = i[1+n(\Omega)] [\chi_{ij}(\vec{x}, \vec{x}'; \Omega+i\eta) - \chi_{ij}(\vec{x}, \vec{x}'; \Omega-i\eta)]. \quad (2.5)$$

Our procedure will be to construct $\chi_{ij}(\vec{x}, \vec{x}'; \Omega \pm i\eta)$ through an equation-of-motion technique, then use Eq. (2.5) to obtain the spectral density that describes the frequency spectrum of spin fluctuations in the sample.

Let \vec{x}_\parallel be the projection of \vec{x} onto a plane parallel to the surface. Then in our semi-infinite geometry, $S_{ij}(\vec{x}, \vec{x}'; \Omega)$ is a function of $\vec{x}_\parallel - \vec{x}'_\parallel$ only, but a function of both y and y' . We exploit the former by writing

$$S_{ij}(\vec{x}, \vec{x}'; \Omega) = \int \frac{d^2Q_\parallel}{(2\pi)^2} S_{ij}(y, y'; \vec{Q}_\parallel, \Omega) e^{i\vec{Q}_\parallel \cdot (\vec{x}_\parallel - \vec{x}'_\parallel)}. \quad (2.6)$$

The function $A_i(\vec{Q}_\parallel, \Omega; y) = S_{ii}(y, y'; \vec{Q}_\parallel, \Omega)$ ($i=x$ or y) has the following physical interpretation. If one examines spin fluctuations in a slab of thickness dy with sides parallel to the surface, with the slab

a distance y below the surface, then $A_i(\vec{Q}_{\parallel}, \Omega; y)$ measures the square of the amplitude of the Fourier component with wave vector \vec{Q}_{\parallel} and frequency Ω of the thermal fluctuation in $S_i(\vec{x}, t)$ within the slab. It is this quantity we study below in our analysis of the frequency spectrum of the DE wave.

In the spin-wave regime, we have interest in only the form functions $\chi_{ij}(\vec{x}, \vec{x}'; t - t')$ with i and j equal to x and y . While we can work directly with the form in Eq. (2.2) and the equations of motion of the appropriate Heisenberg operators, we choose to proceed through resort to a classical method that produces identical results, for excitations of the spin system on a length scale long compared to the lattice constant.

If our spin system is subjected to a magnetic field $\vec{h}_T(\vec{x}, t)$ with origin to be specified below, the Cartesian component of spin density $S_i(\vec{x}, t)$ obeys the equation of motion (we have $\hbar=1$)

$$\frac{\partial S_i(\vec{x}, t)}{\partial t} = \mu [\vec{S}(\vec{x}, t) \times \vec{h}_T(\vec{x}, t)]_i, \quad (2.7)$$

or for the \hat{x} and \hat{y} components explicitly

$$\frac{\partial S_x(\vec{x}, t)}{\partial t} = \mu S_y(\vec{x}, t) h_{T_z}(\vec{x}, t) - M_s h_{T_y}(\vec{x}, t), \quad (2.8a)$$

$$\frac{\partial S_y(\vec{x}, t)}{\partial t} = M_s h_{T_x}(\vec{x}, t) - \mu S_x(\vec{x}, t) h_{T_z}(\vec{x}, t). \quad (2.8b)$$

Here in the spirit of spin-wave theory, we replace $S_z(\vec{x}, t)$ by the constant nS , with n the density of spins and note $\mu nS = M_s$ is the saturation magnetization. We have set $\mu = g\mu_B$.

The magnetic field $\vec{h}_T(\vec{x}, t)$ is composed of a sum of three contributions: (i) The Zeeman field \vec{H} applied along \hat{z} , and an exchange field of strength $-D\nabla^2$, also aligned along \hat{z} . (ii) The demagnetizing field $\vec{h}_d(\vec{x}, t)$ set up by the spin motion. (iii) An externally applied field $\vec{h}_e(\vec{x}, t)$ which varies in space and time.

Upon noting that the components of \vec{h}_d are linear in $S_x(\vec{x}, t)$ and $S_y(\vec{x}, t)$ and neglecting terms in the equations of motion nonlinear in these components, then adding a transverse relaxation time τ , we have

$$\frac{\partial S_x}{\partial t} + \frac{1}{\tau} S_x + M_s h_{d_x} - \mu(H - D\nabla^2) S_y = -M_s h_{e_y}, \quad (2.9a)$$

$$\frac{\partial S_y}{\partial t} + \frac{1}{\tau} S_y - M_s h_{d_x} + \mu(H - D\nabla^2) S_x = +M_s h_{e_x}. \quad (2.9b)$$

The demagnetizing field $\vec{h}_d(\vec{x}, t)$ is given accurately by the magnetostatic approximation, since disturbances in the spin system propagate slowly compared to the velocity of light. Thus, $\nabla \times \vec{h}_d = 0$ and we have $\vec{h}_d = -\nabla\phi$. In addition, we require $\nabla \cdot \vec{h}_d + 4\pi\mu\vec{\nabla} \cdot \vec{S} = 0$. The last statements combined with Eqs. (2.9) lead us to the set of three equations

$$\frac{\partial S_x}{\partial t} + \frac{1}{\tau} S_x - \mu(H - D\nabla^2) S_y - M_s \frac{\partial \phi}{\partial y} = -M_s h_{e_y}, \quad (2.10a)$$

$$\frac{\partial S_y}{\partial t} + \frac{1}{\tau} S_y + \mu(H - D\nabla^2) S_x + M_s \frac{\partial \phi}{\partial x} = M_s h_{e_x}, \quad (2.10b)$$

and

$$\nabla^2 \phi - 4\pi\mu \frac{\partial S_x}{\partial x} - 4\pi\mu \frac{\partial S_y}{\partial y} = 0. \quad (2.10c)$$

These equations, supplemented by boundary conditions described below, will form the basis of the present analysis. It is useful to rewrite these in a more abstract but more compact notation. Define new variables $u_1 = S_x$, $u_2 = S_y$, and $u_3 = \phi$. Then let $f_1 = +M_s h_{e_y}$, $f_2 = -M_s h_{e_x}$, and $f_3 = 0$. Suppose we give $h_{e_y}(\vec{x}, t)$ the time variation $\exp(-i\Omega t)$, with the same time variation for $S_x(\vec{x}, t)$ and $S_y(\vec{x}, t)$. Finally, we introduce the matrix of differential operators L_{ij} where, with $\bar{\Omega} = \Omega + i/\tau$,

$$L = \begin{bmatrix} +i\bar{\Omega} & \mu(H - D\nabla^2) & M_s \frac{\partial}{\partial y} \\ -\mu(H - D\nabla^2) & +i\bar{\Omega} & -M_s \frac{\partial}{\partial x} \\ -4\pi\mu \frac{\partial}{\partial x} & -4\pi\mu \frac{\partial}{\partial y} & \nabla^2 \end{bmatrix}. \quad (2.11)$$

Then with this convention, the information contained in (2.10) may be expressed in the simple form

$$\sum_{j=1}^3 L_{ij}(\vec{x}) u_j(\vec{x}) = f_i(\vec{x}). \quad (2.12)$$

The formal solution of these equations is achieved by introducing an array of Green's functions $g_{ij}(\vec{x}, \vec{x}'; \Omega)$ that satisfy

$$\sum_{k=1}^3 L_{ik}(\vec{x}) g_{kj}(\vec{x}, \vec{x}'; \Omega) = \delta_{ij} \delta(\vec{x} - \vec{x}').$$

One has

$$u_i(\vec{x}) = \sum_{j=1,2} \int d^3x' g_{ij}(\vec{x}, \vec{x}'; \Omega) f_j(\vec{x}'), \quad (2.13)$$

where in Eq. (2.13) recall $f_3(\vec{x}) = 0$ by definition.

By comparing Eq. (2.13) with Eq. (2.1), the Green's functions directly give $\chi_{ij}(\vec{x}, \vec{x}'; \Omega)$, the Fourier transform of $\chi_{ij}(\vec{x}, \vec{x}'; t - t')$. One readily notes the identities

$$\chi_{xx}(\vec{x}, \vec{x}'; \Omega) = -nSg_{12}(\vec{x}, \vec{x}'; \Omega), \quad (2.14a)$$

$$\chi_{xy}(\vec{x}, \vec{x}'; \Omega) = +nSg_{11}(\vec{x}, \vec{x}'; \Omega), \quad (2.14b)$$

$$\chi_{yx}(\vec{x}, \vec{x}'; \Omega) = -nSg_{22}(\vec{x}, \vec{x}'; \Omega), \quad (2.14c)$$

and

$$\chi_{yy}(\vec{x}, \vec{x}'; \Omega) = +nSg_{21}(\vec{x}, \vec{x}'; \Omega). \quad (2.14d)$$

So far we have said little about the boundary conditions for our problem. With \vec{x}' fixed inside the sample (or outside the sample), quite clearly from Eq. (2.13) the elements $g_{1j}(\vec{x}, \vec{x}'; \Omega)$ of the Green's-function array, considered as functions of \vec{x} , obey the same boundary conditions as the \hat{x} component of spin density $\mathfrak{S}_x(\vec{x}, t)$. Similarly, when considered as functions of \vec{x} for fixed \vec{x}' , $g_{2j}(\vec{x}, \vec{x}'; \Omega)$ obeys the same boundary conditions as $\mathfrak{S}_y(\vec{x})$ while $g_{3i}(\vec{x}, \vec{x}'; \Omega)$ the same as $\varphi(\vec{x})$. Thus, continuity of $\varphi(\vec{x})$ across the surface (this ensures continuity of tangential components of \vec{h}) requires

$$g_{3i}(0+, \vec{x}'; \Omega) = g_{3i}(0-, \vec{x}'; \Omega), \quad (2.15a)$$

while conservation of normal (\hat{y}) components of $\vec{h} + 4\pi n\mu\vec{S}$ (normal \vec{b}) gives

$$\left(-\frac{\partial g_{3i}}{\partial y} + 4\pi\mu g_{2i}\right)_{\vec{x}=0+} = -\left(\frac{\partial g_{3i}}{\partial y}\right)_{\vec{x}=0-}. \quad (2.15b)$$

The boundary condition on the magnetization components \mathfrak{S}_x and \mathfrak{S}_y at the surface requires a brief discussion. If one considers a semi-infinite lattice of spins coupled by exchange interactions of short range, then the boundary condition becomes²⁰ $\hat{n} \cdot \vec{\nabla}\mathfrak{S}_x = 0$ and $\hat{n} \cdot \vec{\nabla}\mathfrak{S}_y = 0$ at the surface, where \hat{n} is a unit vector normal to the surface. In practice, this is an oversimplified description of the boundary condition. Spins at the surface often experience effective-pinning fields which inhibit their motion. A diverse variety of extrinsic and intrinsic mechanisms can give rise to effective-pinning fields. With this in mind, we take the boundary conditions on the transverse magnetization at the surface to have the form

$$\left(\frac{\partial g_{1i}}{\partial y} - \lambda g_{1i}\right)_{\vec{x}=0+} = 0 \quad (2.16a)$$

and

$$\left(\frac{\partial g_{2i}}{\partial y} - \lambda g_{2i}\right)_{\vec{x}=0+} = 0, \quad (2.16b)$$

where λ is a phenomenological parameter that provides a measure of the strength of the surface pinning field. If $\lambda = 0$, we recover the zero-slope boundary condition appropriate to slowly varying disturbances in the semi-infinite Heisenberg ferromagnet, while if we let $\lambda \rightarrow \infty$, the boundary condition becomes $\mathfrak{S}_x = \mathfrak{S}_y = 0$ at the surface. This corresponds to the limit of very strong surface pinning, with motion of the surface spins fully inhibited by the surface pinning.

In contrast to the other parameters of our theory, which may all be deduced from known bulk properties of a given material, λ is sensitive to the microscopic details of the surface geometry. To illustrate this, consider a semi-infinite fcc lattice of spins with a (100) surface and nearest-neighbor exchange interactions J . Let the spins in the outermost atomic layer experience an effective pinning field of strength H_s parallel to the external Zeeman field. Then by taking the long-wavelength limit of the appropriate equations of motion, one finds $\lambda = \mu H_s a_0 / 2D$ with a_0 the lattice constant and $D = a_0^2 S J$ the bulk-spin-wave exchange stiffness. Thus, λ is influenced by the environment of the outermost atomic layer of spins. We note that it has recently been proposed that magnetic reconstruction acting in concert with surface-anisotropy fields can produce pinning parameters λ with a strong dependence on both temperature and magnetic field.⁵

Our boundary condition in Eq. (2.16) is appropriate to the case where the Zeeman field is aligned along a high-symmetry direction in the surface layer. Then symmetry considerations ensure the surface pinning field is either parallel ($\lambda > 0$) or possibly antiparallel ($\lambda < 0$) to the Zeeman field. In general, this need not be so, with the consequence that the spins near the surface may cant relative to the Zeeman field. An analysis of this surface spin canting, including quantitative contact with the data of Wigen and his co-workers,⁷ has been presented by Hirada, Nagai, and Nagamiya,¹⁰ and also by Stakelon.¹⁰

We are now in a position to find the explicit form of the Green's functions $g_{ij}(\vec{x}, \vec{x}'; \Omega)$. If the equations are written out explicitly, one obtains three distinct sets, each of which couples three elements of the Green's matrix together. We discuss explicitly the set that couples $g_{11}(\vec{x}, \vec{x}'; \Omega)$, $g_{21}(\vec{x}, \vec{x}'; \Omega)$, and $g_{31}(\vec{x}, \vec{x}'; \Omega)$. We then simply quote the results of the set $g_{i2}(\vec{x}, \vec{x}'; \Omega)$ and we shall have no interest here in the set $g_{i3}(\vec{x}, \vec{x}'; \Omega)$.

We begin by Fourier transforming out the dependence on \vec{x}_\parallel and \vec{x}'_\parallel :

$$g_{ij}(\vec{x}, \vec{x}'; \Omega) = \int \frac{d^2 Q_\parallel}{(2\pi)^2} g_{ij}(y, y'; \vec{Q}_\parallel, \Omega) \exp[i\vec{Q}_\parallel \cdot (\vec{x}_\parallel - \vec{x}'_\parallel)]. \quad (2.17)$$

In what follows, in the interest of compactness, we suppress explicit reference to \vec{Q}_\parallel and Ω in $g_{ij}(y, y'; \vec{Q}_\parallel, \Omega)$.

The three functions $g_{i1}(y, y'; \vec{Q}_\parallel, \Omega)$ satisfy the equations, with $h = H + DQ_\parallel^2$,

$$\begin{aligned} &+ i\bar{\Omega} g_{11}(y, y') + \mu \left(h - D \frac{\partial^2}{\partial y^2} \right) g_{21}(y, y') \\ &+ \mu M_s \frac{\partial}{\partial y} g_{31}(y, y') = \delta(y - y'), \quad (2.18a) \end{aligned}$$

$$-\mu \left(h - D \frac{\partial^2}{\partial y^2} \right) g_{11}(y, y') + i\tilde{\Omega} g_{21}(y, y') - i\mu M_s Q_x g_{31}(y, y') = 0, \quad (2.18b)$$

$$+ 4\pi\mu i Q_x g_{11}(y, y') + 4\pi\mu \frac{\partial}{\partial y} g_{21}(y, y') + \left(Q_{\parallel}^2 - \frac{\partial^2}{\partial y^2} \right) g_{31}(y, y') = 0. \quad (2.18c)$$

A convenient way to proceed with the solution of Eqs. (2.18) is to introduce an auxiliary function $\Lambda_1(y, y')$ related to the three Green's functions in the following manner:

$$g_{11}(y, y') = \left[i\tilde{\Omega} \left(Q_{\parallel}^2 - \frac{\partial^2}{\partial y^2} \right) + 4\pi i \mu M_s Q_x \frac{\partial}{\partial y} \right] \Lambda_1(y, y'), \quad (2.19a)$$

$$g_{21}(y, y') = \left[4\pi\mu M_s Q_x^2 + \mu \left(h - D \frac{\partial^2}{\partial y^2} \right) \left(Q_{\parallel}^2 - \frac{\partial^2}{\partial y^2} \right) \right] \Lambda_1(y, y'), \quad (2.19b)$$

and

$$g_{31}(y, y') = \mu \left[4\pi\tilde{\Omega} Q_x - 4\pi\mu \left(h - D \frac{\partial^2}{\partial y^2} \right) \frac{\partial}{\partial y} \right] \Lambda_1(y, y'). \quad (2.19c)$$

One may verify that for any choice of $\Lambda_1(y, y')$, the two homogeneous members of Eqs. (2.18) are satisfied automatically, while Eq. (2.18a) requires

$$\left[\mu^2 \left(h - D \frac{\partial^2}{\partial y^2} \right)^2 \left(Q_{\parallel}^2 - \frac{\partial^2}{\partial y^2} \right) - \tilde{\Omega}^2 \left(Q_{\parallel}^2 - \frac{\partial^2}{\partial y^2} \right) + 4\pi\mu^2 M_s \left(h - D \frac{\partial^2}{\partial y^2} \right) \left(Q_x^2 - \frac{\partial^2}{\partial y^2} \right) \right] \Lambda_1(y, y') = \delta(y - y'). \quad (2.20)$$

The homogeneous version of Eq. (2.20) is satisfied if the dependence of $\Lambda_1(y, y')$ on y assumes the form $\exp(i\kappa y)$, where κ is any root of the equation

$$\mu^2 (h + D\kappa^2)^2 (Q_{\parallel}^2 + \kappa^2) - \tilde{\Omega}^2 (Q_{\parallel}^2 + \kappa^2) + 4\pi\mu^2 M_s (h + D\kappa^2) (Q_x^2 + \kappa^2) = 0. \quad (2.21)$$

Equation (2.21) is a cubic in κ^2 which yields three distinct solutions we write as κ_i^2 , $i = 1, 2, \text{ or } 3$. By κ_i we mean a root of Eq. (2.21) subject to the constraint

$$\text{Im}(\kappa_i) > 0. \quad (2.22)$$

In the presence of a nonzero relaxation time τ , for real \tilde{Q}_{\parallel} and $\tilde{\Omega}$, all roots of Eq. (2.21) have non-

zero imaginary parts. We can always select three roots κ_i with positive imaginary parts as a consequence.

We need to solve the inhomogeneous version of Eq. (2.20). First suppose we consider an infinitely extended medium, where $\Lambda_1(y, y')$ is necessarily a function of $y - y'$. (Here and below we confine attention to the case $y' > 0$.) We then write

$$\Lambda_1(y, y') = \Lambda_1^{(\infty)}(y - y') = \int_{-\infty}^{+\infty} \frac{d\kappa}{2\pi} e^{i\kappa(y-y')} \Lambda_1^{(\infty)}(\kappa), \quad (2.23)$$

where substitution into Eq. (2.20) gives

$$\Lambda_1^{(\infty)}(\kappa) = \frac{1}{D^2} \frac{1}{(\kappa^2 - \kappa_1^2)(\kappa^2 - \kappa_2^2)(\kappa^2 - \kappa_3^2)}. \quad (2.24)$$

The contour integral in Eq. (2.23) is then evaluated, with the requirement $\Lambda_1^{(\infty)} \rightarrow 0$ as $|y - y'| \rightarrow \infty$. This gives

$$\Lambda_1^{(\infty)}(y - y') = \frac{i}{2D^2} \sum_{i=1}^3 \epsilon_i \exp(i\kappa_i |y - y'|), \quad (2.25)$$

where

$$\epsilon_1 = [\kappa_1(\kappa_1^2 - \kappa_2^2)(\kappa_1^2 - \kappa_3^2)]^{-1}, \quad (2.26)$$

and ϵ_2, ϵ_3 are formed by cyclic permutation of the indices on the right-hand side of Eq. (2.26). It will be useful to note the identities

$$\sum_{i=1}^3 \kappa_i \epsilon_i = 0, \quad (2.27a)$$

and also

$$\sum_{i=1}^3 \kappa_i^3 \epsilon_i = 0. \quad (2.27b)$$

The Green's functions generated by inserting Eq. (2.25) into Eqs. (2.19) satisfy Eqs. (2.18), but they fail to satisfy the boundary conditions at the surface. This we handle by adding to $\Lambda_1^{(\infty)}(y - y')$ solutions to the homogeneous version of Eq. (2.20), with coefficients to be adjusted to satisfy the boundary conditions. Thus, we write, for $y > 0$

$$\Lambda_1(y, y') = \frac{i}{2D^2} \left(\sum_{i=1}^3 \epsilon_i e^{i\kappa_i |y - y'|} + \sum_{i=1}^3 \alpha_i e^{+i\kappa_i y} \right). \quad (2.28)$$

where we shall find the α_i to be functions of y' .

Outside the crystal, for $y < 0$, $g_{11}(y, y')$ and $g_{21}(y, y')$ necessarily vanish simply because there is no magnetization there. This is not true of $g_{31}(y, y')$ for $y' > 0$, since the driven spins necessarily set up a magnetic field outside the crystal. The requirement that $\nabla \cdot \vec{h}_d = 0$ outside the crystal

dictates that (for $y' > 0$) $g_{31}(y, y') = \alpha_0 \exp(Q_{\parallel} y)$. Thus we have the four constants α_0 and $\alpha_1 - \alpha_3$ that are uniquely determined from the boundary conditions.

We shall not describe the details of the algebra, but we simply present the results of our analysis. We define the three quantities

$$\gamma_{1i}(\pm) = -\frac{1}{2D^2} [\bar{\Omega}(Q_{\parallel}^2 + \kappa_i^2) \pm 4\pi i \mu M_s Q_x \kappa_i], \quad (2.29a)$$

$$M = \begin{bmatrix} (i\kappa_1 - \lambda)\gamma_{11}(+) & (i\kappa_2 - \lambda)\gamma_{12}(+) & (i\kappa_3 - \lambda)\gamma_{13}(+) \\ (i\kappa_1 - \lambda)\gamma_{21} & (i\kappa_2 - \lambda)\gamma_{22} & (i\kappa_3 - \lambda)\gamma_{23} \\ (i\kappa_1 - Q_{\parallel})\gamma_{31}(+) - 4\pi\gamma_{21} & (i\kappa_2 - Q_{\parallel})\gamma_{32}(+) - 4\pi\gamma_{22} & (i\kappa_3 - Q_{\parallel})\gamma_{33}(+) - 4\pi\gamma_{23} \end{bmatrix}. \quad (2.30)$$

We also introduce

$$\Gamma_{1i} = (i\kappa_i + \lambda)\gamma_{1i}(-)\epsilon_i, \quad (2.31a)$$

$$\Gamma_{2i} = (i\kappa_i + \lambda)\gamma_{2i}\epsilon_i, \quad (2.31b)$$

$$\Gamma_{3i} = [(i\kappa_i + Q_{\parallel})\gamma_{3i}(-) + 4\pi\gamma_{2i}]\epsilon_i. \quad (2.31c)$$

Then we find the coefficients α_i in Eq. (2.28) may be written

$$\alpha_i = \sum_{j=1}^3 \sum_{k=1}^3 M_{ij}^{-1} \Gamma_{jk} e^{i\kappa_k y'}, \quad (2.32a)$$

$$\equiv \sum_{k=1}^3 A_{ik} e^{i\kappa_k y'}, \quad (2.32b)$$

where

$$A_{ik} = \sum_{j=1}^3 M_{ij}^{-1} \Gamma_{jk}. \quad (2.32c)$$

In terms of the quantities defined above,

$$g_{11}(y, y') = \sum_{i=1}^3 \gamma_{1i}(\pm)\epsilon_i e^{i\kappa_i |y-y'|} + \sum_{i=1}^3 \sum_{j=1}^3 \gamma_{1i}(+) A_{ij} e^{i\kappa_i y} e^{i\kappa_j y'}, \quad (2.33a)$$

$$g_{21}(y, y') = \sum_{i=1}^3 \gamma_{2i}\epsilon_i e^{i\kappa_i |y-y'|} + \sum_{i=1}^3 \sum_{j=1}^3 \gamma_{2i} A_{ij} e^{i\kappa_i y} e^{i\kappa_j y'}, \quad (2.33b)$$

$$\gamma_{2i} = \frac{i}{2D^2} [\mu(h + D\kappa_i^2)(Q_{\parallel}^2 + \kappa_i^2) + 4\pi\mu M_s Q_x^2], \quad (2.29b)$$

and

$$\gamma_{3i}(\pm) = \frac{\mu}{2D^2} [4\pi i \bar{\Omega} Q_x \pm 4\pi\kappa\mu(h + D\kappa_i^2)], \quad (2.29c)$$

and then set up the matrix M given by

and

$$g_{31}(y, y') = \sum_{i=1}^3 \gamma_{3i}(\pm)\epsilon_i e^{i\kappa_i |y-y'|} + \sum_{i=1}^3 \sum_{j=1}^3 \gamma_{3i}(+) A_{ij} e^{i\kappa_i y} e^{i\kappa_j y'}. \quad (2.33c)$$

The forms in Eq. (2.34) are valid for both $y > 0$ and $y' > 0$. By the notation

$$\gamma_{ji}(\pm) \exp(i\kappa_i |y - y'|)$$

we mean $\gamma_{ji}(+)\exp[i\kappa_i(y - y')]$ when $y > y'$ and $\gamma_{ji}(-)\exp[-i\kappa_i(y - y')]$ when $y < y'$. We remark that it is the identities in Eqs. (2.27) which ensure that no δ functions appear in the Green's functions, when the differentiations in Eqs. (2.19) are carried through.

By means of a similar procedure, one may obtain expressions for $g_{12}(y, y')$, $g_{22}(y, y')$, and $g_{32}(y, y')$. As remarked earlier, in the interests of brevity, we omit the details and give only the final results.

Here we introduce

$$\delta_{1i} = -\frac{i}{2D^2} [\mu(h + D\kappa_i^2)(Q_{\parallel}^2 + \kappa_i^2) + 4\pi\mu M_s \kappa_i^2], \quad (2.34a)$$

$$\delta_{2i}(\pm) = -\frac{1}{2D^2} [\bar{\Omega}(Q_{\parallel}^2 + \kappa_i^2) \mp 4\pi i \mu M_s Q_x \kappa_i], \quad (2.34b)$$

$$\delta_{3i}(\pm) = -\mu \frac{2\pi}{D^2} [Q_x \mu(h + D\kappa_i^2) \mp i \bar{\Omega} \kappa_i], \quad (2.34c)$$

and the matrix

$$P = \begin{bmatrix} (i\kappa_1 - \lambda)\delta_{11} & (i\kappa_2 - \lambda)\delta_{12} & (i\kappa_3 - \lambda)\delta_{13} \\ (i\kappa_1 - \lambda)\delta_{21}(+) & (i\kappa_2 - \lambda)\delta_{22}(+) & (i\kappa_3 - \lambda)\delta_{23}(+) \\ (i\kappa_1 - Q_{\parallel})\delta_{31}(+) - 4\pi\delta_{21}(+) & (i\kappa_2 - Q_{\parallel})\delta_{32}(+) - 4\pi\delta_{22}(+) & (i\kappa_3 - Q_{\parallel})\delta_{33}(+) - 4\pi\delta_{23}(+) \end{bmatrix}. \quad (2.35)$$

Also, let

$$\Delta_{1i} = (i\kappa_i + \lambda)\delta_{1i}\epsilon_i, \quad (2.36a)$$

$$\Delta_{2i} = (i\kappa_i + \lambda)\delta_{2i}(-)\epsilon_i, \quad (2.36b)$$

$$\Delta_{3i} = [(i\kappa_i + Q_{||})\delta_{3i}(-) + 4\pi\delta_{2i}(-)]\epsilon_i, \quad (2.36c)$$

and finally

$$B_{ij} = \sum_{k=1}^3 P_{ik}^{-1} \Delta_{kj}. \quad (2.37)$$

Then we have the results, for $y > 0$ and $y' > 0$,

$$g_{12}(y, y') = \sum_{i=1}^3 \delta_{1i}\epsilon_i e^{i\kappa_i|y-y'|} + \sum_{i=1}^3 \sum_{j=1}^3 \delta_{1i} B_{ij} e^{i\kappa_i y} e^{i\kappa_j y'}, \quad (2.38a)$$

$$g_{22}(y, y') = \sum_{i=1}^3 \delta_{2i}(\pm)\epsilon_i e^{i\kappa_i|y-y'|} + \sum_{i=1}^3 \sum_{j=1}^3 \delta_{2i}(+) B_{ij} e^{i\kappa_i y} e^{i\kappa_j y'}, \quad (2.38b)$$

and

$$g_{32}(y, y') = \sum_{i=1}^3 \delta_{3i}(\pm)\epsilon_i e^{i\kappa_i|y-y'|} + \sum_{i=1}^3 \sum_{j=1}^3 \delta_{3i}(+) B_{ij} e^{i\kappa_i y} e^{i\kappa_j y'}. \quad (2.38c)$$

This completes the construction of the response functions that form the basis of the numerical calculations reported in Secs. III and IV of the present paper. We conclude with two important technical comments on the above material.

First of all, through direct examination of the Fourier transform of the response function $\chi_{ij}(\vec{x}, \vec{x}'; t - t')$ defined in Eq. (2.2), one may demonstrate that

$$\chi_{ij}(\vec{x}, \vec{x}'; \Omega - i\eta) = [\chi_{ji}(\vec{x}', \vec{x}; \Omega + i\eta)]^*. \quad (2.39)$$

This identity will prove useful in Secs. III and IV. For instance, from Eq. (2.5) with $i = j$, we can now write

$$S_{ii}(\vec{x}, \vec{x}'; \Omega) = -2[1 + n(\Omega)] \text{Im}[\chi_{ii}(\vec{x}, \vec{x}'; \Omega + i\eta)], \quad (2.40)$$

so we need not explicitly take the discontinuity across the real axis to calculate the diagonal elements of the spectral density of the spin fluctuations.

The second point concerns the behavior of the relaxation time $1/\tau$ introduced into the equations of motion of the spin system. While the presence of this quantity allows us to represent the effect

of dissipation in the spin system phenomenologically, there is a subtle feature of introducing this parameter which requires explicit comment.

In a proper microscopic theory of the spin response, $1/\tau$ will emerge as the imaginary part of an appropriately defined proper self-energy. As a consequence, it will be a function of frequency (and wave vector also, but for our purposes the wave vector may be set to zero). As we move parallel to the real axis in the Ω plane, use of a proper frequency variation of τ^{-1} will modify our numerical results, but the consequences of neglecting this are not serious for our purposes. It is, however, quite crucial to realize that the proper self-energy whose imaginary part yields τ^{-1} has a *branch cut* along the real axis. As we cross the real axis, the imaginary part of the proper self-energy changes sign. The choice of sign chosen for τ here ($\tau > 0$) corresponds to presuming Ω lies just *above* the real axis in the Ω plane. If we were to move *below* the real axis, as when we apply Eq. (2.5), it is necessary to note that $\tau^{-1}(\Omega - i\eta) = -\tau^{-1}(\Omega + i\eta)$. If this feature of $1/\tau(\Omega)$ is not acknowledged, then the Fourier transforms $\chi_{ij}(\vec{x}, \vec{x}'; \Omega)$ constructed from the Green's functions above fail to satisfy the identity in Eq. (2.40). In our numerical work, we have never had to be concerned with this issue, since we always use Eq. (2.40) to express all physical results in terms of $\chi_{ij}(\vec{x}, \vec{x}'; \Omega)$ evaluated above the real axis in the complex Ω plane. As far as we know, this may be done for any physical process one wishes to study. The properties of τ^{-1} in the complex Ω plane are then of no concern.

III. NUMERICAL STUDIES OF THE RESPONSE OF THE SPIN SYSTEM NEAR THE SURFACE

In Sec. I, and also in Sec. II [just after Eq. (2.6)], we introduced a spectral density function $A_i(\vec{Q}_{||}, \Omega; y)$, where the subscript i refers to either y (the direction normal to the surface), or x (parallel to the surface but perpendicular to the magnetization). The physical interpretation of $A_i(\vec{Q}_{||}, \Omega; y)$ is also given after Eq. (2.6). In this section, we present a summary of our numerical studies of the spectral density function $A_x(\vec{Q}_{||}, \Omega; y)$ that characterizes the spectral composition of spin fluctuations parallel to the surface. As we shall see, from this study, we can obtain a clear physical insight into a number of properties of the Damon-Eshbach surface spin wave in the presence of exchange, and on general aspects of the response of the spin system near the crystal surface. We present information only on $A_x(\vec{Q}_{||}, \Omega; y)$; a study of $A_y(\vec{Q}_{||}, \Omega; y)$ yields virtually the same information.

We present the results by introducing convenient dimensionless variables. Distance from the surface is measured in units of $Q_{||}$, i.e., a dimensionless measure of distance from the surface is the variable $\xi = Q_{||}y$. Frequency is measured in units of μH . We do this by setting $\Omega = \mu H \omega$ with ω dimensionless. The influence of exchange is measured by $\omega_x = DQ_{||}^2/\mu H$, and the parameter $\gamma = (\mu H \tau)^{-1}$ governs the relaxation rate of the spin system in dimensionless units. We have set $\gamma = 0.01$ for all calculations reported below, unless noted otherwise. We are left only with $4\pi M_s$, and we have set $r = 4\pi M_s/H = 7.0$ in the calculations described here. Also, in the figures displayed below, the influence of the Bose-Einstein function $[1 + n(\Omega)]$ has been ignored. We also set $\lambda = 0$, and ignore surface spin pinning, save for calculations reported near the end of the discussion.

In Fig. 2, for a variety of propagation angles θ in Fig. 1, we show the spectral density function $A_x(\vec{Q}_{||}, \Omega; y)$ at the surface, with $y = 0$. In Fig. 2, we have taken $\omega_x = 0.01$. Each prominent peak in Fig. 2 is the Damon-Eshbach mode. We see very little other structure in the spectral density at the surface, although one should note the background upon which each DE peak sits. There is no structure at all in the frequency regime $\mu H \leq \Omega \leq \mu(HB)^{1/2}$ where bulk spin waves occur, in the absence of exchange. Thus, the long-wavelength surface-spin response is controlled entirely by

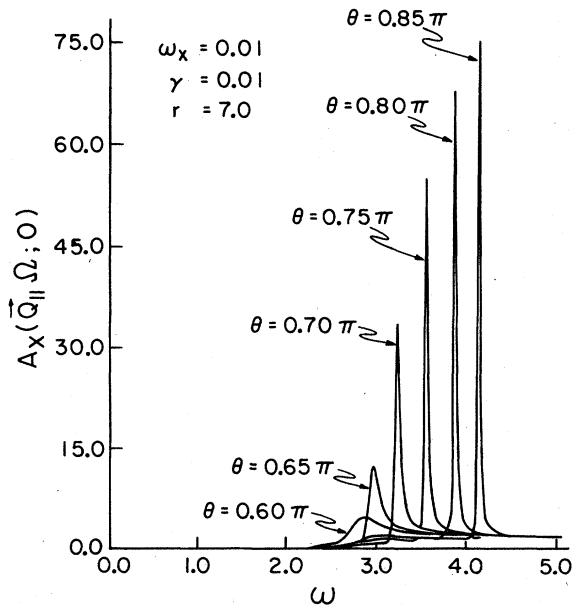


FIG. 2. Spectral density function $A_x(\vec{Q}_{||}, \Omega; y)$ at the surface $y=0$ for $\omega_x = 0.01$ and various propagation angles. Here and in the subsequent figures, the units of $A_x(\vec{Q}_{||}, \Omega; y)$ are arbitrary.

the DE wave, when ω_x is small. The peak positions in Fig. 2 are given quite accurately by the relation

$$\Omega_{DE} = \frac{1}{2} \mu |H/\cos\theta + B \cos\theta|, \quad (3.1)$$

which applies in the limit of zero exchange.

As remarked in Sec. I, the critical angle beyond which no surface-wave propagation occurs is $\theta_c = \pi \pm \psi_c$, where $\psi_c = \cos^{-1}[(H/B)^{1/2}]$. That is, propagation occurs only when θ lies in the range from $\pi + \psi_c$ to $\pi - \psi_c$. In the present instance $\psi_c = 0.38$, so $\theta_c = 0.62\pi, 1.38\pi$ for our parameters. The curves in Fig. 2 provide a vivid picture of how the DE wave "disappears" as the critical propagation angle is approached. First note that as θ_c is approached from within the allowed range of propagation angles, the DE peak broadens. With the small amount of exchange present, these waves are in fact leaky-surface waves, with lifetime limited by radiation of energy into the bulk in addition to the damping described by τ^{-1} . For most of the angles in Fig. 2, the width of the DE feature is controlled by τ^{-1} and the radiative leak is of great quantitative importance. But as θ_c is approached, the DE frequency sinks toward $\Omega_M = \mu(HB)^{1/2}$ and the radiative leak increases, with the consequence that the DE peak broadens as θ approaches θ_c from within the range of allowed angles. In essence, the surface wave anticipates its upcoming merger with the bulk-spin-wave continuum appropriate to zero exchange. When $\theta = 0.6\pi$, a value beyond $\theta_c = 0.62\pi$, we see a broad but nonetheless clear resonance at a frequency below Ω_M . The surface mode has disappeared, but a resonance level in the bulk continuum appears in the spectral density. The integrated strength of the Damon-Eshbach peak also decreases monotonically as θ approaches θ_c from within the range of propagation angles allowed for the surface waves.

From the angular variation of the linewidth, and the integrated strength of the DE wave at the surface, we obtain an intuitive feeling for the way in which the mode gradually and continuously disappears as θ disappears as θ_c is approached. As ω_x is decreased, so does the angular range over which the wave "dissolves" into the bulk continuum through radiation damping.

We next turn to a study of the variation of the spectral function $A_x(\vec{Q}_{||}, \Omega; y)$ with distance from the surface. We do this for $\theta = 0.7\pi$, $\omega_x = 0.01$, and various values of $\xi = Q_{||}y$. For ξ as small as 0.1 [Fig. 3(a)], there is considerable structure in the spectral density not present at $\xi = 0$, although the DE peak remains the dominant feature in the response. At $\xi = 0.5$ [Fig. 3(b)], dramatic oscillatory structure appears, although $A_x(\vec{Q}_{||}, \Omega; y)$ is always positive definite as required by general con-

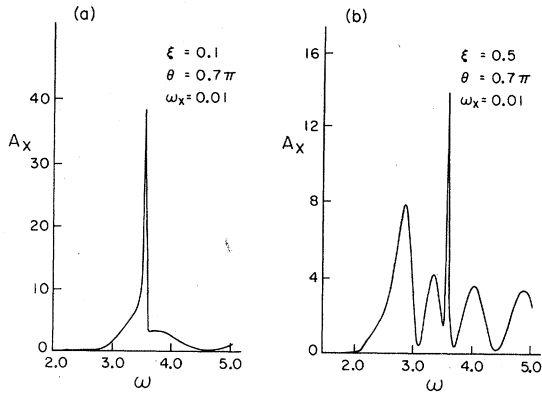


FIG. 3. Behavior of $A_x(\vec{Q}_{\parallel}, \Omega; y)$ with $\xi = Q_{\parallel}y$ for the propagation angle $\theta = 0.7\pi$ and (a) $\xi = 0.1$ and (b) $\xi = 0.5$.

siderations. The DE peak remains a strong feature in the spectral density, though it no longer dominates its integrated strength.

The oscillatory structure in Fig. 3(b) has its origin in the fact that in the presence of exchange, any solution of the spin equations of motion is a linear combination $\sum_i s_i \exp(i\kappa_i y)$, where the κ_i are the roots of the secular equation (2.21). In the frequency regime where the large oscillations are evident in Fig. 3(b), at least one of the κ_i has large real part, and the κ_i depend on frequency. This produces interference beats in the spectral density. As we penetrate more deeply, since y becomes larger, and the κ_i vary with frequency, the interference oscillations become very rapid as one scans frequency. We illustrate this in Fig. 4(a), where we plot the spectral density for $\theta = 0.7\pi$ and $\xi = 5.0$. The DE peak is missing by now, but a very fine interference pattern remains.

Upon increasing y , these oscillations become ever more rapid but decrease in amplitude until one

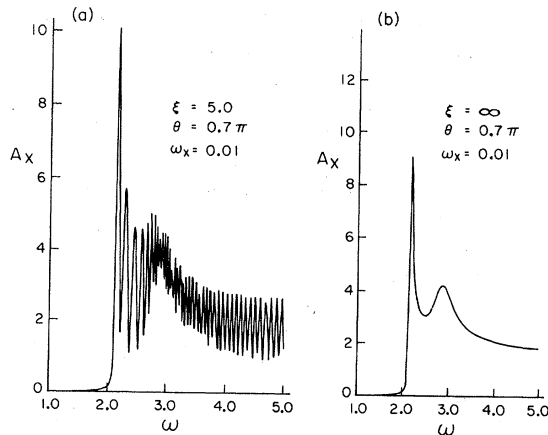


FIG. 4. Behavior of $A_x(\vec{Q}_{\parallel}, \Omega; y)$ with $\xi = Q_{\parallel}y$ for $\theta = 0.7\pi$ and (a) $\xi = 5.0$ and (b) $\xi = \infty$.

achieves the bulk spectral density $A_x(\vec{Q}_{\parallel}, \Omega; y = \infty)$ displayed in Fig. 4(b). In this spectrum, one sees a sharp peak just above the *minimum* bulk-spin-wave frequency Ω_m allowed for this angle, and a second structure just above the maximum bulk-spin-wave frequency Ω_M . The shifts away from Ω_m and Ω_M and the prominent high-frequency tail on the bulk spectral density both arise from the influence of exchange, which allows all frequencies above Ω_M to be present in the spin fluctuations, and not just those between Ω_m and Ω_M as one finds in the absence of exchange. We shall hear more of this high-frequency tail in Sec. V where we discuss Sandercock's light-scattering study of spin excitations at the surface of an Fe film.

We return to a study of the spectral density at the surface, to see the influence of increasing the effect of exchange, through increasing the parameter $\omega_x = DQ_{\parallel}^2/\mu H$.

In Fig. 5(a), we show the surface spectral density $A_x(\vec{Q}_{\parallel}, \Omega; 0)$ for the same propagation angles used in Fig. 2, but now with $\omega_x = 0.1$ rather than $\omega_x = 0.01$. The Damon-Eshbach peaks are very much broader than in Fig. 2, illustrating that for this value of ω_x , radiation damping is the dominant source of linewidth for *all* angles of propagation, not just those near the critical angle θ_c . We have tested this by runs for various values of the dimensionless damping parameter γ , to see that the structures in Fig. 5(a) are indeed insensitive to γ , for γ in the vicinity of 0.01. Note that near θ_c , even though $\omega_x = 0.1$ is a small amount of exchange energy in the wave, the DE peaks are very broad, and the mode ill defined. We also call attention to the absolute magnitude of $A_x(\vec{Q}_{\parallel}, \Omega; 0)$. The peak in the spectral density is broadened, and the peak value is lowered. Finally, a measurement of the peak positions in Fig. 5(a) shows them upshifted in frequency compared to Fig. 2. From these shifts, we may plot the frequency of the DE wave as a function of ω_x . We pre-

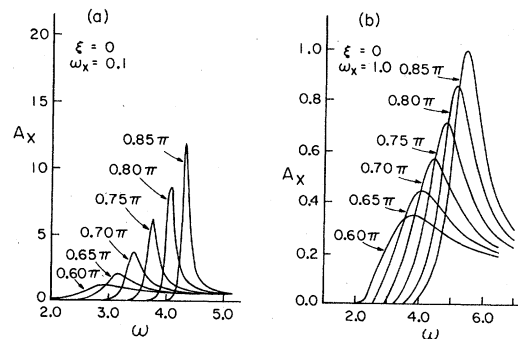


FIG. 5. Behavior of $A_x(\vec{Q}_{\parallel}, \Omega; 0)$ for various propagation angles, and (a) $\omega_x = 0.10$ and (b) $\omega_x = 1.0$.

sent this information below.

In Fig. 5(b), we give the DE response for $\omega_x = 1.0$. The peaks are now very broad and highly asymmetric; the asymmetry in the DE peak is also clearly evident in the curves calculated for smaller values of ω_x , although here we see it easily. The DE peaks are now sufficiently broad, with radiation damping dominant, that their lifetime is only a few oscillation periods.

Through analysis of a sequence of plots such as those presented above, we have extracted the dependence of the frequency and width of the DE surface spin wave on wave vector, for various propagation angles. For this purpose, we use as the operational definition of the frequency of the mode the position of the peak in the spectral density $A_x(\vec{Q}_{\parallel}, \Omega; 0)$, and we define the linewidth to be the full width at half maximum. Because of the clear asymmetry present in the DE peaks, it is an oversimplification to condense the information contained in the spectral density into two such parameters, although we can convey trends compactly by this procedure. We note that the analysis through use of the equation-of-motion method presented by Wolfram and de Wames¹⁴ contains the implicit assumption that the DE feature in the spectral density is a fully symmetric Lorentzian.

In Fig. 6, for three angles of propagation we show the frequency of the Damon-Eshbach wave as a function of its wave vector for three angles of propagation. The solid line represents our empirical dispersion relation extracted from the spectral density plots from the procedure outlined above. The dimensionless units of wave vector are $q = (D/\mu H)^{1/2} Q_{\parallel}$. In Fig. 6, the circles repre-

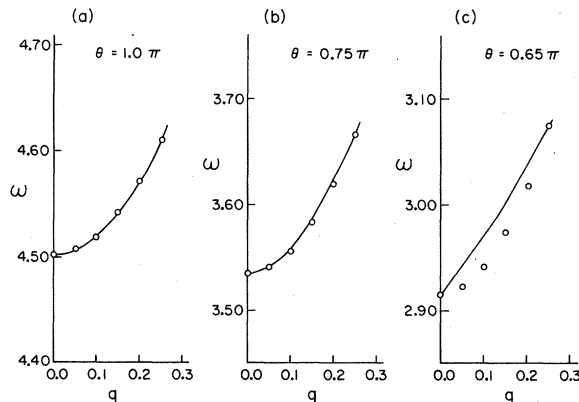


FIG. 6. Frequency of the Damon-Eshbach wave (reduced units) as a function of its wave vector (reduced units). The dimensionless wave vector is $q = (D/\mu_B H)^{1/2} Q_{\parallel}$. We show three propagation directions: (a) $\theta = 1.0\pi$, (b) $\theta = 0.75\pi$, and (c) $\theta = 0.65\pi$. The circles describe points on a parabola fitted to the calculated dispersion relation (solid line) at $q = 0.25$.

sent points on a parabolic dispersion relation $\omega(q) = \omega(0) + D'q^2$, with D' chosen to fit the empirical dispersion relation at $q = 0.25$. For propagation perpendicular to the magnetization ($\theta = \pi$), our dispersion relation is accurately fitted by the parabolic law with $D' = 1.76$, in good agreement with Wolfram and de Wames' analytic result.¹³ However, for $\theta = 0.65\pi$ near the critical angle θ_c , the parabolic law provides a poor fit. Close inspection of the numerical results shows $\omega(q) - \omega(0)$ varies linearly with q at small q , with curvature at larger values. For the intermediate angle $\theta = 0.75\pi$, we find a reasonable fit with the parabolic law with $D' = 2.10$; there is a small but nonetheless significant discrepancy between the solid curve and the parabolic law.

In Fig. 7, we show the variation of linewidth with frequency of the surface wave, for the three propagation angles in Fig. 6. We see the dramatic increase in linewidth from radiative damping as the critical angle is approached. We remind the reader that we have set the relaxation time τ introduced in Sec. II so the parameter $\gamma = 1/\mu_B H \tau$ assumes the value 0.01. At $q = 0$, where $\omega(q) = \omega(0)$, the lifetime of the DE wave is controlled by the relaxation time, but radiation damping sets in with increasing strength as q increases.

The information on the dispersion relation and the width of the Damon-Eshbach peak summarized in Figs. 6 and 7 was obtained by fixing the value of \vec{Q}_{\parallel} , then scanning the frequency Ω . One can equally well define an effective dispersion relation by fixing the frequency Ω , then scanning the wave vector \vec{Q}_{\parallel} . Such a procedure is relevant to the following experiment. Imagine driving the surface spins by placing a line source of magnetic field parallel to the surface, and close to it. If the mag-

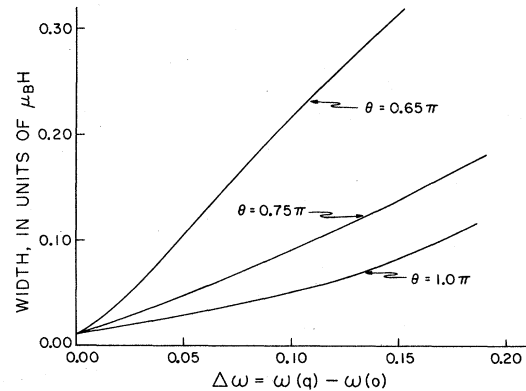


FIG. 7. For the three angles examined in Fig. 6, we give the width of the Damon-Eshbach wave as a function of frequency. The spin-damping parameter γ has been chosen equal to 0.01.

netic field oscillates in time with frequency Ω , then the response of the spin system measured "downstream" from the line source is found by convoluting the spectral densities $A_i(\vec{Q}_{\parallel}, \Omega; 0) \exp(i\vec{Q}_{\parallel} \cdot \vec{x}_{\parallel})$ with coupling constants that are functions of \vec{Q}_{\parallel} . Here \vec{Q}_{\parallel} is directed normal to the line source of field. Viewed from an equation-of-motion approach analogous to that used by Wolfram and de Wames,¹⁴ the experiment discussed above would probe the real and imaginary parts of \vec{Q}_{\parallel} that emerge from an equation-of-motion analysis with Ω real. The imaginary part of \vec{Q}_{\parallel} gives the attenuation length of a disturbance set up by an oscillating line source of magnetic field near the surface. The real part of \vec{Q}_{\parallel} controls the period of the spatial oscillations that are functions of \vec{Q}_{\parallel} .

We have constructed the real and imaginary parts of \vec{Q}_{\parallel} for several propagation angles, by scanning $A_x(\vec{Q}_{\parallel}, \Omega; 0)$ with Ω fixed, and the magnitude of \vec{Q}_{\parallel} scanned through the Damon-Eshbach peak. The peak is again asymmetric, as before, so this may be done meaningfully only for modest values of $\omega - \omega(0)$. We find the effective dispersion relation obtained in this way quantitatively very close to those in Fig. 6, save for $\theta = 0.65\pi$ where significant quantitative differences are evident. Near the critical angle, the features in the spectral density are skewed sufficiently that a unique dispersion relation cannot be defined. We note that $\text{Im}(Q_{\parallel})$, obtained from the width of the peak in the spectral density, is of the same order as $\text{Re}(Q_{\parallel})$ so that the wave is severely attenuated. This is true even when ω_x is small, and this occurs because in the absence of exchange, the frequency of the wave is independent of the magnitude of \vec{Q}_{\parallel} . With a small bit of exchange added, for fixed real Ω , an equation-of-motion approach (explored explicitly by us) shows $\text{Re}(\vec{Q}_{\parallel})$ and $\text{Im}(\vec{Q}_{\parallel})$ the same order of magnitude even for small ω_x .

The calculations discussed in the present section have presumed the pinning parameter $\lambda \equiv 0$, so the "zero-slope" boundary condition is imposed on both components of the transverse magnetization. In Fig. 8, we show the effect of spin pinning on the spectral density, for two values of ω_x and a sequence of pinning parameters λ . This is done here for only one propagation angle, $\theta = 0.7\pi$, but the results displayed are typical of those obtained for other angles. For $\lambda > 0$, as explained earlier, the surface-anisotropy field acts to "pin" the surface spins and inhibit their response. For $\lambda < 0$, considered also in Fig. 8, the effective-surface-anisotropy field is antiparallel to the Zeeman field, so spins in the surface see a smaller total effective field than spins in the bulk.

From Fig. 8, we see that as λ is increased in the positive sense, the Damon-Eshbach peaked is

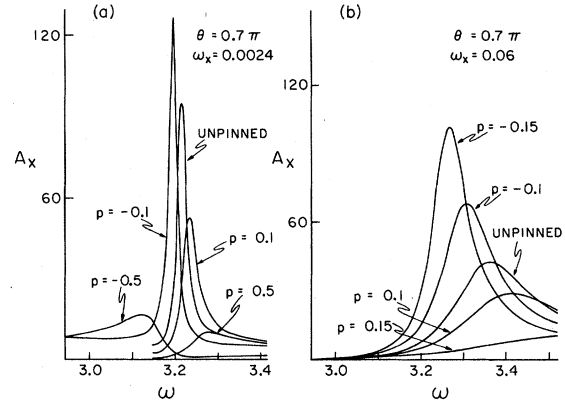


FIG. 8. For $\theta = 0.7\pi$ and the two values of ω_x indicated, we show the effect of spin pinning on ω_x . The dimensionless parameter $p = \lambda (D/\mu_B H)^{1/2}$.

shifted up in frequency, and its amplitude diminished, as expected on physical grounds. It is also broadened substantially, with the broadening eventually severe enough to cause the surface spin spectral density to become rather featureless.

The physical origin of the broadening is clear. If the parameter ω_x is small, then one of the decay constants κ_i lies close to the value $i|\vec{Q}_{\parallel}|$ expected in the presence of only dipolar coupling. The remaining two roots are large in absolute magnitude, and necessarily move off to infinity in the limit $\omega_x \rightarrow 0$. For $\theta = \pi$, this is evident from the analytic results displayed by Wolfram and de Wames, and it remains true for other angles as well. If the surface-spin pinning is increased and the amplitude of the transverse magnetization in the DE wave driven to zero at the surface, a value far from that expected from the solution with only dipolar coupling present, one must mix in the two "exchange-wave" solutions with large κ_i to make the magnetization vanish. One of these waves is responsible for the radiation leak to the interior, so as forcing the magnetization to zero increases its amplitude, the radiative leak to the interior increases.

For $\lambda < 0$, the DE wave softens, as expected. The peak initially *narrows* as $|\lambda|$ increases, to eventually broaden until the DE feature in the spectral density is washed out, very much as in the case of $\lambda > 0$.

This concludes our discussion of the basic properties of the response of the spin system in the near vicinity of the crystal surface. While the spectral-density functions displayed here provides a vivid picture of the response in the surface region, unfortunately they cannot be probed directly. Sections IV and V are devoted to light scattering from magnetic surfaces, with emphasis on the recent very beautiful experimental studies.

IV. SCATTERING OF LIGHT BY SPIN WAVES ON FERROMAGNETIC SURFACES

In this section, we develop the theory of the inelastic scattering of light by spin waves at the surface of a semi-infinite crystal. We shall then apply the theory to scattering from the surface of EuO and Fe, to make contact with the results reported by Grünberg and Metawe⁸ (EuO) and by Wettling and Sandercock⁹ (Fe). The theory presented here gives a good account of the angle variation of the intensity of light scattered by the Damon-Eshbach wave, and also of other features of the data. Before we enter the theoretical discussion, a few general remarks are in order.

In the experiments, as in numerous light-scattering studies of surfaces, the frequency of the laser light lies in an absorption band. In the case of EuO, the laser frequency lies beyond the absorption edge, in a frequency region where we estimate the skin depth to be 1500 Å. In Fe, under the laser excitation used by Wettling and Sandercock, the skin depth is around 150 Å. Thus, one observes light backscattered from the surface, as illustrated in Fig. 9. Since the scattering volume is small, scattering from bulk excitations is small, and features specific to the surface appear in the spectrum. The surface waves appear on equal footing with bulk waves, for example. In the present section, we are concerned with scattering by spin waves that have frequencies in the range of a few cm^{-1} , which is the frequency regime appropriate to Brillouin spectroscopy.

We believe the light-scattering method offers a

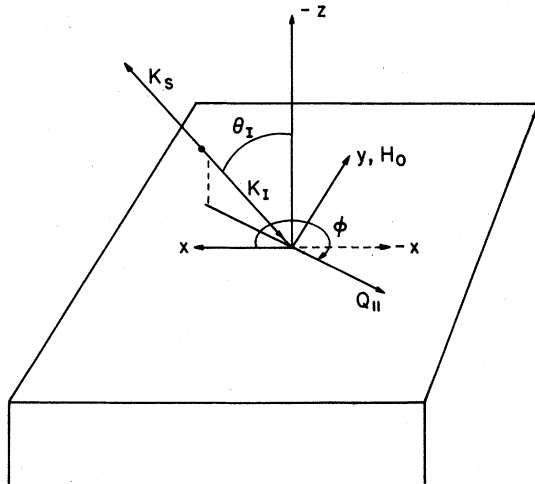


FIG. 9. Experimental geometry. Light is incident at an angle θ_I with the normal. The scattered light collected is that backscattered in the direction of the incident beam. The magnitude of the transfer wave vector parallel to the surface, $|\vec{Q}_{II}|$, equals $(|K_I| + |K_S|)\sin\theta_I$. Experimentally only $\varphi = 0$ or $\varphi = 180$ have been studied.

potentially powerful and flexible probe of magnetic surfaces, under conditions where direct contact is possible with theories of magnetic surface response, as we shall see from the analysis below. We compare briefly the light-scattering method with the more traditional ferromagnetic-resonance studies of thin films or spheroidal samples.

In ferromagnetic-resonance studies, the wavelength of the incident microwave radiation is usually larger than typical sample dimensions. Thus, one always excites modes that are geometrical resonances of the whole sample,²¹ rather than modes appropriate to the conceptually much simpler semi-infinite geometry. From resonance studies, it is thus difficult to obtain information specific to a particular surface orientation, without resort to a carefully prepared sample of planar geometry. Unfortunately, while the films used in standing-spin-wave studies in ferromagnetic resonance have this planar geometry, they are usually polycrystalline and complicated by the presence of a non-magnetic substrate. The mode structure is thus equally influenced by the nature of the film-substrate interface as it is by the film-vacuum interface. Finally, the microwave cavities used in resonance studies operate typically at one, or at best, a small number of frequencies. Data taken with only a single frequency is often hard to interpret in an unambiguous manner.⁵

The light-scattering method uses a probe with wavelength small compared to sample sizes. The method can in principle probe the carefully prepared single-crystal surfaces through use of radiation with wavelength very short compared to sample size. Thus, one has a tool that can examine a crystalline surface, under conditions that closely approximate the semi-infinite geometry. One can also vary the externally applied magnetic field *continuously*, and follow its influence on the modes without being restricted to one or a discrete number of frequencies. In both experiments cited above, the Damon-Eshbach and bulk-spin-wave features in the spectrum have been followed over a wide range of magnetic fields.

We now turn to the light-scattering theory we have developed, based on the correlation functions derived and studied in Secs. II and III. Before we do, a comment on the choice of coordinate axes may avoid confusion. In Sec. II, where the theory of the surface response of the spin system was developed, the \hat{z} axis was directed along the magnetization (parallel to the surface), while the \hat{y} axis was directed normal to the surface. This was done since in the magnetism literature, the \hat{z} axis is conventionally aligned along the magnetization. Here we wish to discuss light scattering from the surface, with help from the Green's-

function apparatus erected for earlier theories of light scattering from surfaces and films.⁵ To use the Green's functions described in these papers directly, it is useful to orient the \hat{z} axis normal to the crystal, with crystal in the upper half space, as shown in Fig. 9. Thus the present section uses the axes displayed in Fig. 9, with magnetization directed along \hat{y} . Some care must be exercised when using the specific forms in Sec. II in the formulas here, as noted explicitly below.

The light couples to spin waves in the material because modulation of the spin density $\vec{S}(\vec{x}, t)$ by thermal fluctuations leads to modulation of the dielectric tensor $\epsilon_{\mu\nu}$ by terms first order in $S_\mu(\vec{x}, t)$. In addition, the fluctuating magnetic field $\vec{h}_d(\vec{x}, t)$ associated with the thermal motion of the spins also modulates the dielectric tensor. To first order in these quantities, we write the fluctuating part $\delta\epsilon_{\mu\nu}(\vec{x}, t)$ of the dielectric tensor in the form

$$\delta\epsilon_{\mu\nu}(\vec{x}, t) = \sum_\lambda K_{\mu\nu\lambda} S_\lambda(\vec{x}, t) + \sum_\lambda P_{\mu\nu\lambda} h_{d\lambda}(\vec{x}, t), \quad (4.1)$$

where $K_{\mu\nu\lambda}$ is the change in $\epsilon_{\mu\nu}$ caused by reorientation of the magnetization, with zero magnetic field, and $P_{\mu\nu\lambda}$ the change in $\epsilon_{\mu\nu}$ by application of a magnetic field, with magnetization held fixed. The time and spatial variations of $\vec{S}(\vec{x}, t)$ and $\vec{h}_d(\vec{x}, t)$ are sufficiently slow that $K_{\mu\nu\lambda}$ and $P_{\mu\nu\lambda}$ are well approximated by the form appropriate to static, spatially uniform changes in \vec{S} and \vec{h}_d . However, both are functions of the incident-light frequency, and for our purposes the difference in frequency between the incident and scattered light is small.

In the treatment below, we ignore $P_{\mu\nu\lambda}$ by setting it to zero, since we expect it to be small compared to $K_{\mu\nu\lambda}$. This may be justified by a simple physical argument,²² and our confidence in this assumption is bolstered further by the good agreement we find for the angular variation of the ratio of the cross section for scattering from the Damon-Eshbach wave, and for scattering from bulk spin waves.

The nonzero elements of the tensor $K_{\mu\nu\lambda}$ may be obtained from symmetry arguments,²³ noting the transformation properties of $S_\lambda(\vec{x}, t)$ under time reversal and spatial rotations are identical to a magnetic field. For a cubic material we have

$$K_{\mu\nu\lambda} = K\epsilon_{\mu\nu\lambda}, \quad (4.2)$$

where $\epsilon_{\mu\nu\lambda}$ is the Levi-Civita tensor, and the prefactor K becomes purely imaginary for a transparent material, but is in general complex.

The comments above confine attention to terms linear in the spin density $S_\mu(\vec{x}, t)$. It has been pointed out²⁴ that below T_c terms quadratic in the

spin density also contribute to the one-spin-wave scattering. The influence of these terms is ignored for the moment in the interest of simplicity. We comment again on them at the end of the section, where the modifications of the formulas derived from Eq. (4.2) produced by the quadratic terms will be given.

With the above introductory remarks in hand, the theory of light scattering from the surface proceeds along the lines outlined in Ref. 15. In the interest of brevity, we do not repeat the full definitions of all quantities that enter the analysis, but instead we refer the reader to Ref. 15.

The scattered field below the material may be written in terms of the Green's functions $D_{\alpha\beta}(\vec{x}, \vec{x}'; t - t')$ of the Maxwell equations. In Ref. 15, the explicit forms of the Green's functions are given for a three-layer geometry. We quote below the special limiting form of these functions appropriate to the present problem. If $E_\alpha^{(s)}(\vec{x}, t)$ is the α th Cartesian coordinate of the scattered electric field, $E_\alpha^{(0)}(\vec{x}, t)$ that of the incident field inside the medium, and ω_0 the frequency of the incoming light, we have¹⁵

$$E_\alpha^{(s)}(\vec{x}, t) = \left(\frac{\omega_0}{c}\right)^2 \sum_{\beta\gamma} \int \frac{d^3x' dt'}{4\pi} D_{\alpha\beta}(\vec{x}, \vec{x}'; t - t') \times \delta\epsilon_{\beta\gamma}(\vec{x}', t') E_\gamma^{(0)}(\vec{x}', t'), \quad (4.3)$$

where here we write the incident field in the medium in the form

$$E_\gamma^{(0)}(\vec{x}', t') = \sum_\eta T_{\gamma\eta} E_\eta^{(0)} \exp(i\vec{k}_\parallel^{(0)} \cdot \vec{x}'_\parallel + ik_{1\perp}^{(0)} z - i\omega_0 t). \quad (4.4)$$

In Eq. (4.4), $E_\eta^{(0)}$ is the amplitude of the η th Cartesian component of the incident electric field outside the crystal, and $T_{\gamma\eta}$ is a matrix of transmission coefficients with $\sum_\eta T_{\gamma\eta} E_\eta^{(0)}$ the γ th Cartesian component of incident electric just inside the crystal at $z = 0+$. The wave vector $\vec{k}_\parallel^{(0)}$ is the projection of the wave vector of the incident light on a plane parallel to the surface. The magnitude of $\vec{k}_\parallel^{(0)}$ is $(\omega_0/c) \sin\theta_I$, with θ_I the incident angle illustrated in Fig. 9. Finally $k_{1\perp}^{(0)}$ is the complex wave vector of the incident light in the crystal. If ϵ is its complex dielectric constant, and c the velocity of light in vacuum,

$$k_{1\perp}^{(0)} = (\omega_0/c)(\epsilon - \sin^2\theta_I)^{1/2}, \quad \text{Im}(k_{1\perp}^{(0)}) > 0. \quad (4.5)$$

Through use of the procedures in Ref. 15, one may form an expression for the Brillouin-scattering efficiency per unit solid angle, per unit frequency interval. We write $E_\eta^{(0)} = E^{(0)} \hat{n}_\eta$ with \hat{n}_η a unit vector, and recall the definition of $\epsilon_{\alpha\beta}(\vec{k}_\parallel, \omega|z)$ to obtain the differential scattering efficiency $d^2S/d\omega_s d\Omega(\hat{k}_s)$ in the form

$$\begin{aligned} \frac{d^2S}{d\omega_s d\Omega(\hat{k}_s)} &= \frac{\cos\theta_s}{8\pi^3} \left(\frac{\omega_0}{c}\right)^6 \sum_{\alpha} \sum_{\beta\gamma\eta} \sum_{\beta'\gamma'\eta'} \sum_{\delta\delta'} T_{\gamma\eta} T_{\gamma'\eta'}^* \hat{n}_{\eta} \hat{n}_{\eta'} K_{\beta'\gamma'\delta'}^* K_{\beta\gamma\delta} \\ &\times \int_0^{\infty} dz' \int_0^{\infty} dz'' \epsilon_{\alpha\beta}(\vec{k}_{\parallel}^{(s)}, \omega_s | z') \epsilon_{\alpha\beta}^*(\vec{k}_{\parallel}^{(s)}, \omega_s | z'') \\ &\times \exp(ik_{1z}^{(0)} z' - ik_{1z}^{(0)*} z'') \\ &\times \int d^2r_{\parallel} \int dt \exp[i(\Omega t - \vec{Q}_{\parallel} \cdot \vec{r}_{\parallel})] \langle S_{\delta}(\vec{r}_{\parallel}, z''; \tau) S_{\delta}(0, z'; 0) \rangle. \end{aligned} \quad (4.6)$$

In Eq. (4.6), $\Omega = \omega_0 - \omega_s$ is the change in frequency of the light upon scattering, and $\vec{Q} = \vec{k}_{\parallel}^{(0)} - \vec{k}_{\parallel}^{(s)}$ is the projection of the change in wave vector of the light onto the plane parallel to the surface. Note that \vec{Q}_{\parallel} is necessarily real.

We turn to the form of $\epsilon_{\alpha\beta}(\vec{k}_{\parallel}, \omega | z)$. In Ref. 15, these functions were constructed for a substrate that occupied the half space $z < 0$, a film in the region $0 < z < d$, and vacuum in the region $d < z$. We obtain the form of these functions in the form appropriate to the present geometry by letting $d \rightarrow \infty$, replacing the dielectric constant of the substrate by unity, and that of the film by the (complex) quantity ϵ . We write for $z' > 0$

$$\epsilon_{\alpha\beta}(\vec{k}_{\parallel}^{(s)}, \omega_s | z') = (c/i\omega_0) \Gamma_{\alpha\beta}(\vec{k}_{\parallel}^{(s)}, \omega_0) \exp(ik_{1z}^{(s)} z') \quad (4.7)$$

and

$$k_{1z}^{(s)} = (\omega_0/c)(\epsilon - \sin^2\theta_s)^{1/2}, \quad \text{Im}(k_{1z}^{(s)}) > 0, \quad (4.8)$$

and again we ignore the difference between the frequency of the incident and scattered light. The tensor $\Gamma_{\alpha\beta}(\vec{k}_{\parallel}^{(s)}, \omega_0)$ is readily expressed in terms of two quantities $\gamma_s(\theta_s)$ and $\gamma_p(\theta_s)$. Let

$$k_{1z}^{(s)} = \frac{\omega_0}{c} \cos\theta_s \quad (4.9)$$

be the magnitude of the normal component of the wave vector of the scattered radiation below the crystal²⁵ and define

$$\gamma_s(\theta) = (\omega_0/c)(k_{1z}^{(s)} + k_{1z}^{(s)})^{-1}, \quad (4.10a)$$

$$\gamma_p(\theta) = (c/\omega_0)k_{1z}^{(s)}k_{1z}^{(s)}(k_{1z}^{(s)} + \epsilon k_{1z}^{(s)})^{-1}. \quad (4.10b)$$

Then if $k_{\parallel x}^{(s)} = k_{\parallel}^{(s)} \cos\varphi_s$ and $k_{\parallel y}^{(s)} = k_{\parallel}^{(s)} \sin\varphi_s$ defines the azimuthal angle φ_s , we have²⁵

$$\Gamma_{xx}(\vec{k}_{\parallel}^{(s)}, \omega_s) = \cos^2\varphi_s \gamma_p(\theta_s) + \sin^2\varphi_s \gamma_s(\theta_s), \quad (4.11a)$$

$$\begin{aligned} \Gamma_{xy}(\vec{k}_{\parallel}^{(s)}, \omega_s) &= \Gamma_{yx}(\vec{k}_{\parallel}^{(s)}, \omega_s) \\ &= \sin\varphi_s \cos\varphi_s [\gamma_p(\theta_s) - \gamma_s(\theta_s)], \end{aligned} \quad (4.11b)$$

$$\Gamma_{xz}(\vec{k}_{\parallel}^{(s)}, \omega_s) = \cos\varphi_s (k_{1z}^{(s)}/k_{1z}^{(s)}) \gamma_p(\theta_s), \quad (4.11c)$$

$$\Gamma_{zx}(\vec{k}_{\parallel}^{(s)}, \omega_s) = \cos\varphi_s (k_{1z}^{(s)}/k_{1z}^{(s)}) \gamma_p(\theta_s), \quad (4.11d)$$

$$\Gamma_{yz}(\vec{k}_{\parallel}^{(s)}, \omega_s) = \sin\varphi_s (k_{1z}^{(s)}/k_{1z}^{(s)}) \gamma_p(\theta_s), \quad (4.11e)$$

$$\Gamma_{zy}(\vec{k}_{\parallel}^{(s)}, \omega_s) = \sin\varphi_s (k_{1z}^{(s)}/k_{1z}^{(s)}) \gamma_p(\theta_s), \quad (4.11f)$$

$$\Gamma_{yy}(\vec{k}_{\parallel}^{(s)}, \omega_s) = \sin^2\varphi_s \gamma_p(\theta_s) + \cos^2\varphi_s \gamma_s(\theta_s), \quad (4.11g)$$

$$\Gamma_{zz}(\vec{k}_{\parallel}^{(s)}, \omega_s) = (k_{1z}^{(s)2}/k_{1z}^{(s)}k_{1z}^{(s)}) \gamma_p(\theta_s). \quad (4.11h)$$

Then we introduce

$$F_{\delta\delta}(\vec{k}_0, \vec{k}_s; \Omega) = \int d^2r_{\parallel} \int dt dz' dz'' \exp(i\Delta k_{1z} z' - i\Delta k_{1z}^* z'') \exp[i(\Omega t - \vec{Q}_{\parallel} \cdot \vec{r}_{\parallel})] \langle S_{\delta}(\vec{r}_{\parallel}, z''; t) S_{\delta}(0, z'; 0) \rangle \quad (4.12)$$

with

$$\Delta k_{1z} = k_{1z}^{(0)} + k_{1z}^{(s)} \quad (4.13)$$

to write the Brillouin scattering efficiency in the form

$$\frac{d^2S}{d\Omega(\hat{k}_s) d\omega_s} = \frac{\cos\theta_s}{8\pi^3} \left(\frac{\omega_0}{c}\right)^4 \sum_{\alpha} \sum_{\beta\gamma\eta} \sum_{\beta'\gamma'\eta'} \sum_{\delta\delta'} T_{\gamma\eta} T_{\gamma'\eta'}^* \hat{n}_{\eta} \hat{n}_{\eta'} K_{\beta'\gamma'\delta'}^* K_{\beta\gamma\delta} \Gamma_{\alpha\beta}(\vec{k}_{\parallel}^{(s)}, \omega_0) \Gamma_{\alpha\beta}^*(\vec{k}_{\parallel}^{(s)}, \omega_0) F_{\delta\delta}(\vec{k}_0, \vec{k}_s; \Omega). \quad (4.14)$$

The expression in Eq. (4.14) provides a general expression for the Brillouin efficiency. We reduce it down to a simpler form, with the experimental geometry of Refs. 8 and 9 in mind. In the scheme of Fig. 9, we presume s-polarized incident radiation, with the x - z plane the plane of incidence, and the incident electric field parallel to the magnetization along \hat{y} . Furthermore, for $K_{\beta\gamma\delta}$ we take the form in Eq. (4.2) appropriate to a cubic crystal. Then with T_s the transmission coefficient of the s-polarized light through the surface, the scattering efficiency becomes

$$\frac{d^2S}{d\Omega(\hat{k}_s) d\omega_s} = \frac{\cos\theta_s}{8\pi^3} \left(\frac{\omega_0}{c}\right)^4 |T_s|^2 |K|^2 \left[|\gamma_s|^2 \sin^2\varphi_s F_{xx} + \frac{|\gamma_p|^2}{\cos^2\theta_s} \left(\cos^2\varphi_s F_{xx} + \frac{(k_{\parallel}^{(s)})^2}{|k_{\perp}^{(s)}|^2} F_{xx} - \frac{k_{\parallel} \cos\varphi_s}{|k_{\perp}^{(s)}|^2} (k_{\perp}^{(s)} F_{xx} + k_{\perp}^{(s)*} F_{xx}) \right) \right]. \quad (4.15)$$

The contribution in Eq. (4.15) from s-polarized scattered radiation is proportional to $|\gamma_s|^2$, while that from p-polarized radiation in the final state is proportional to $|\gamma_p|^2$.

The functions $F_{6\sigma}$, defined in Eq. (4.12) are related to the response functions $\chi_{ij}(\vec{x}, \vec{x}'; \Omega \pm i\eta)$ of Sec. II through the identity

$$F_{6,\delta}(\vec{k}_0, \vec{k}_s; \Omega) = i[1+n(\Omega)] \int d^2r_{\parallel} dz' dz'' \exp(i\Delta k_{\perp} z' - i\Delta k_{\perp}^* z'') \exp(-i\vec{Q}_{\parallel} \cdot \vec{r}_{\parallel}) [\chi_{6,\delta}(\vec{r}_{\parallel}, z'', 0, z'; \Omega + i\eta) - \chi_{6,\delta}(\vec{r}_{\parallel}, z'', 0, z'; \Omega - i\eta)]. \quad (4.16)$$

Through use of the identity in Eq. (2.39), and the definitions

$$r_{\perp, \perp} = |\gamma_s|^2 \sin^2\varphi_s + |\gamma_p|^2 (\cos^2\varphi_s / \cos^2\theta_s), \quad (4.17a)$$

$$r_{\parallel, \parallel} = (k_{\parallel}^{(s)})^2 |\gamma_p|^2 / |k_{\perp}^{(s)}|^2 \cos^2\theta_s, \quad (4.17b)$$

$$r_{\parallel, \perp} = k_{\parallel}^{(s)} \cos\varphi_s |\gamma_p|^2 / |k_{\perp}^{(s)*}| \cos^2\theta_s, \quad (4.17c)$$

we can write

$$\frac{d^2S}{d\Omega(\hat{k}_s) d\omega_s} = \frac{\cos\theta_s}{4\pi^3 i} \left(\frac{\omega_0}{c}\right)^4 |T_s|^2 |K|^2 [1+n(\Omega)] \times \text{Im} \left(\int_0^{\infty} dz' \int_0^{\infty} dz'' \exp(i\Delta k_{\perp} z' - i\Delta k_{\perp}^* z'') [r_{\perp, \perp} \chi_{xx}(\vec{Q}_{\parallel}, \Omega + i\eta; z'', z') - r_{\parallel, \perp} \chi_{xx}(\vec{Q}_{\parallel}, \Omega + i\eta; z'', z') - r_{\parallel, \perp}^* \chi_{xx}(\vec{Q}_{\parallel}, \Omega + i\eta; z'', z') + r_{\parallel, \parallel} \chi_{xx}(\vec{Q}_{\parallel}, \Omega + i\eta; z'', z')] \right). \quad (4.18)$$

When the form of the correlation functions in Sec. II are inserted into Eq. (4.18), the integral on z'' and z' is elementary. We thus obtain a rather complicated, but nonetheless closed analytic expression for the light-scattering cross section. Upon feeding in the complex dielectric constant of the substrate, along with information on the scattering geometry and magnetic parameters of the substrate, we are able to sweep out the Brillouin spectrum, and examine it for evidence of the phenomena described in Sec. III. The result in Eq. (4.18) forms the basis for the numerical calculations reported below. We remind the reader of the difference between coordinate system used in the present section, and in Sec. II. One translates between the two by noting that the coordinate axis normal to the surface is y in Sec. II while here it is z . Then we have the following table:

$$\chi_{zz}(\text{Sec. IV}) \equiv \chi_{yy}(\text{Sec. II}), \quad (4.19a)$$

$$\chi_{xz}(\text{Sec. IV}) \equiv \chi_{zx}(\text{Sec. II}), \quad (4.19b)$$

$$\chi_{zx}(\text{Sec. IV}) \equiv -\chi_{yx}(\text{Sec. II}), \quad (4.19c)$$

$$\chi_{xz}(\text{Sec. IV}) \equiv \chi_{xz}(\text{Sec. II}). \quad (4.19d)$$

We conclude with remarks on the modification of Eq. (4.18) by the terms quadratic in the spin density. Following Wettling *et al.*,²⁴ one introduces

quadratic terms in the fluctuating part of the dielectric tensor. Thus, Eq. (4.1) is supplemented by adding in

$$\delta\epsilon_{\mu\nu}^{(2)}(\vec{x}, t) = \sum_{\lambda\delta} G_{\mu\nu\lambda\delta} \mathfrak{S}_{\lambda}(\vec{x}, t) \mathfrak{S}_{\delta}(\vec{x}, t). \quad (4.20)$$

These terms contribute to the one-spin-wave cross section by virtue of terms with either λ or δ equal to z , and $\mathfrak{S}_{\lambda}(\vec{x}, t)$ replaced simply by nS . If we introduce these terms into the present discussion, the only terms which enter involve the elements G_{xyxy} and permutations. Upon calling these G_{44} , then the influence of the quadratic terms is introduced by the following replacements in Eq. (4.18):

$$|K|^2 r_{\perp, \perp} \rightarrow |K|^2 r_{\perp, \perp} + 2 \text{Re}(K^* g r_{\perp, \perp}^*) + |g|^2 r_{\parallel, \parallel}, \quad (4.21a)$$

$$|K|^2 r_{\parallel, \parallel} \rightarrow |K|^2 r_{\parallel, \parallel} - 2 \text{Re}(K^* g r_{\parallel, \parallel}^*) + |g|^2 r_{\perp, \perp}, \quad (4.21b)$$

$$-|K|^2 r_{\parallel, \perp} \rightarrow -|K|^2 r_{\parallel, \perp} - K^* g r_{\parallel, \parallel} + g^* K r_{\perp, \perp} + |g|^2 r_{\parallel, \perp}^*, \quad (4.21c)$$

$$-|K|^2 r_{\perp, \parallel} \rightarrow -|K|^2 r_{\perp, \parallel} - K g^* r_{\parallel, \parallel} + K^* g r_{\perp, \perp} + |g|^2 r_{\perp, \parallel}^*. \quad (4.21d)$$

In these equations $g = 2nSG_{44}$.

V. RESULTS OF NUMERICAL STUDIES OF LIGHT SCATTERING FOR MAGNETIC SURFACES

In this section, we present our theoretical results for light scattering from the two materials EuO and Fe, both of which were the topic of the recent experimental studies.^{8,9} As we shall see, the basic parameters that characterize these two systems are dramatically different, and thus provide illustrations of the extremes one may reasonably expect.

The experimental geometry is illustrated in Fig. 9. The light strikes the surface at an angle θ_I with the normal, and plane of incidence is the x - y plane, for the data reported so far. The scattered light collected is that backscattered in the direction of the incident beam. Thus, the magnitude of \vec{Q}_\parallel is $2\omega_0 \sin\theta_I/c$, where ω_0 is the incident frequency. We confine our attention to this geometry here, save for calculations presented near the end of the section which explore the nature of the spectrum when \vec{Q}_\parallel deviates from the direction perpendicular to the magnetization. In the theoretical calculations, we always assume the incident field polarized parallel to the magnetization.

Before we present our results, we comment on trends present in the data common to both systems. These features emerge from our theoretical analysis, as we shall see.

In the light-scattering spectra, the bulk spin waves give rise to a feature that appears on both the Stokes and the anti-Stokes side of the line. The surface spin wave appears on only *one* side, depending on the orientation of the Zeeman field relative to \vec{Q}_\parallel . If the surface wave appears on the anti-Stokes side, reversal of the field direction moves it to the Stokes side. The same happens if \vec{Q}_\parallel is changed in sign by rotating the direction of the incident field about the surface by 180° .

The fact that the surface wave appears on only one side of the line is an elegant demonstration of the nonreciprocity of the dispersion relation. The detailed balancing arguments that assign $\exp(+\hbar\Omega/k_B T)$ as the Stokes to anti-Stokes ratio relate one scattering event to the other by a time-reversal argument. Thus, the Stokes side of the line associated with wave-vector transfer \vec{Q}_\parallel should be compared with the anti-Stokes side of the spectrum at $-\vec{Q}_\parallel$. The Stokes and anti-Stokes portion of the spectrum associated with a *given* wave vector \vec{Q}_\parallel are related by the detailed balancing argument only if $+\vec{Q}_\parallel$ and $-\vec{Q}_\parallel$ are equivalent.

Another feature common to the two sets of data is a strong dependence on incident angle θ_I of the ratio of the integrated intensity of the DE wave to that of the bulk waves. As the angle of incidence increases, the surface-wave feature becomes much more intense, relative to the scattering from the

bulk waves. This result emerges naturally from our calculation.

Before we turn to the detailed results, we point out the difference between EuO and Fe. First of all, the optical skin depths differ by nearly an order of magnitude. In EuO, we estimate the skin depth to be about 1500 Å, for the incident frequency used by Grünberg and Metawe. For Fe illuminated by the same frequency, the skin depth is only 150 Å. The wave vector of the DE wave created is $2\omega_0 \sin\theta_I/c$ in magnitude independent of the skin depth. However, one may expect the bulk waves to have wave vectors normal to the surface as large as δ^{-1} . Thus, in Fe the bulk wave created in the experiment will be influenced much more importantly by exchange than they are in EuO, all other factors presumed identical. Also, since we saw in Sec. III that the spectral density at the surface receives its dominant contribution from the DE wave, the small skin depth of Fe renders scattering from the DE wave much stronger relative to scattering from bulk waves when Fe and EuO are compared.

In fact, Fe has a Curie temperature of ≈ 1050 K compared with the Curie temperature of ≈ 70 K for EuO. The value of the exchange stiffness constant D for Fe is thus very much larger than in EuO. This enhances the influence of exchange on the bulk waves over that expected from the small skin depth, when Fe and EuO are compared. Indeed, the exchange constant of Fe is sufficiently large that we predict observable consequences of exchange on the DE wave, in addition to exchange effects in the bulk-spin-wave portion of the spectrum. Thus, EuO offers us an example of a spectrum where the influence of exchange is small, and in Fe it plays an important role in the data already available, and we predict additional effects discussed below.

Of course, Fe is also a metal, and differs fundamentally from EuO in this sense. The long-wavelength spin waves in a ferromagnet are described by the present formalism, with its description of exchange for metals as well as insulators.²⁶ However, a complete account of the spin response would include eddy-current damping of the spin motion. Our formalism is easily extended to do this, but here we presume the influence of eddy-current damping may be incorporated into our phenomenological relaxation time τ .

We now turn to a more detailed discussion of light scattering from these two materials.

(i) EuO: In Fig. 10, we summarize the results of our theoretical spectra for EuO. We estimate from the literature that at the laser frequency used in the experiment, 5145 Å, we have $n \approx 0.25$ and $\kappa \approx 1.6$, to produce a skin depth of roughly 1500 Å.

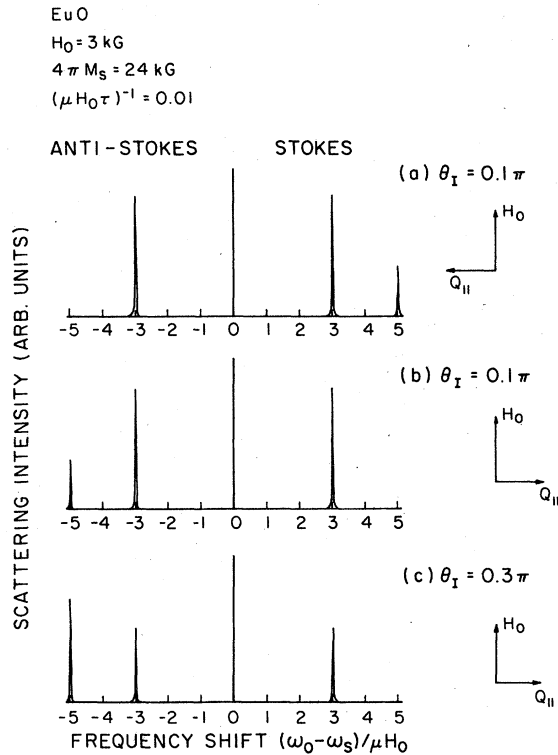


FIG. 10. Theoretical spectra for EuO for a back-scatter measurement. Note that reversing the direction of $Q_{||}$ reverses the side on which the surface wave peak appears.

In the calculations reported here, we have set the parameter g in Eqs. (4.20) equal to zero.

In each of the figures, we see a feature on *both* the Stokes and anti-Stokes side of the laser line associated with scattering from bulk spin waves. A third feature, present on one side but not the other, comes from the Damon-Eshbach wave. Figures 10(a) and 10(b) compare two spectra calculated for identical parameters save for the *sign* of the wave vector transfer $\vec{Q}_{||}$, which differs in the two cases as indicated. In Fig. 10(a), the DE wave appears on the Stokes side, and in Fig. 10(b) it appears on the anti-Stokes side. In both Figs. 10(a) and 10(b), we have $\theta_0 = 0.1\pi$. In Fig. 10(c), we show a spectrum calculated for $\theta_0 = 0.3\pi$. The intensity of the surface spin wave relative to the bulk wave is much stronger in Fig. 10(c) than in the two preceding ones. This angular variation in the relative intensities is consistent with the results of Grünberg and Metawe.

There is one point where our calculations disagree with the data. We find the Stokes to anti-Stokes ratio of the bulk spin wave to be unity, in Fig. 10. The experiments show a substantial asymmetry, with the bulk-wave Stokes to anti-Stokes ratio unaffected by reversal of magnetic field.

However, Grünberg and Metawe find this ratio altered if the polarization of the incoming radiation is changed. From the discussion in Ref. 24, it is evident that the terms quadratic in the spin density neglected here lead to a modification in the Stokes to anti-Stokes ratio of the kind evident in the data.

We have run a few spectra with the parameter g in Eq. (4.20) nonzero, to verify that the Stokes to anti-Stokes ratio of the bulk wave differs from unity when $g \neq 0$, while the angular variation of the total bulk-spin-wave to surface-spin-wave scattering ratio is not changed greatly. We shall report on the effect of the quadratic terms in detail in a separate publication.

For EuO, the exchange interactions in the spin system play a minor role. The surface-wave peak is centered quite close to the frequency in Eq. (3.1) appropriate to the limit of zero exchange, although there is a small exchange-induced upshift. The same is true for the bulk-spin-wave feature, with the bulk wave very near the frequency $\mu(HB)^{1/2}$ appropriate to propagation normal to the magnetization. In the calculations, we have set $\gamma = (\mu H \tau)^{-1} = 0.01$, and find no evidence of radiation broadening in the Damon-Eshbach peak. We shall see that in Fe, for the reasons outlined above, the exchange effects are substantial.

Grünberg and Metawe also find that both the bulk-spin-wave peak and the DE peak lie substantially below the value calculated by inserting the bulk magnetization into the standard formulas. We comment further on this below.

(ii) Fe: In Fig. 11 we present our theoretical results for the spectra of Fe. We have again used $\theta_I = 0.1\pi$. At the frequency of the laser light we have $n = 2.86$, $\kappa = 2.91$ to give a skin depth of about 150 \AA . As a result of this small skin depth, the interactions with the surface spin waves play a larger role in Fe than in EuO. Since there is little asymmetry evident in the Stokes to anti-Stokes ratio of the bulk spin waves, we have set $G_{44} = 0$ in the calculations for Fe. In Fig. 11 we see that, even at $\theta_I = 0.1\pi$, the surface peak dominates the bulk peaks. This contrasts with EuO where in Fig. 10(a) we see the bulk peak has a larger integrated intensity.

As we have mentioned, the exchange constant is much larger in Fe than in EuO. This is reflected in a comparison of the line shapes of the spectra for the two substances. In Fig. 10(b) for EuO we see on the anti-Stokes side two sharp symmetrical peaks, one at the bulk-spin-wave frequency and one at the surface-spin-wave frequency. In Fig. 11 for Fe on the anti-Stokes side we still see these two peaks. However we also see a tail extending from the bulk peak under the surface peak and beyond. This tail is a result of the exchange interac-

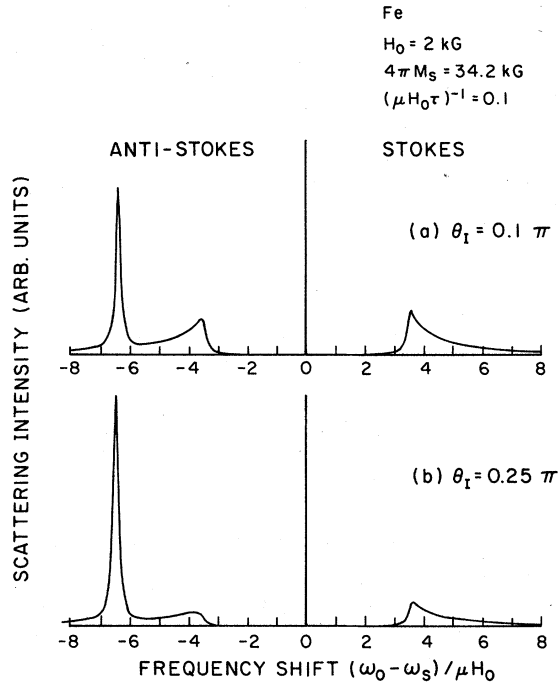


FIG. 11. Theoretical spectra for Fe for a backscatter measurement.

tion extending the bulk-spin-wave band to higher frequencies, as we saw in Fig. 4(b). Thus the frequency region where light scattering occurs also increases. This tail is not seen in the experimental results on EuO since there the effect of exchange is small. However in the experimental work of Sandercock and Wettling on Fe this high-frequency tail is prominent.

We also find from our theoretical study of Fe that the position of both the bulk- and surface-spin-wave peaks are shifted to higher frequencies relative to their values in the limit of no exchange. This shift is consistent with our results in Sec. IV where we saw the position of the DE peak in the spectral density shifted to higher frequencies when exchange energy became important. We find for the parameters used here that the shift in the position of the bulk peak is larger than that for the surface peak. This can be seen in Table I.

TABLE I. Position of the bulk and surface peak as a function on incident angle. ω_0 and ω_s are the incident and scattered frequencies. In the absence of exchange the bulk peak should appear at 3.19 and the surface peak at 5.59 and these positions would be independent of θ_I .

θ_I	Bulk peak $(\omega_0 - \omega_s)/\mu H_0$	Surface peak $(\omega_0 - \omega_s)/\mu H_0$
0.1π	3.25	5.60
0.25π	3.44	5.65
0.4π	3.60	5.71

TABLE II. Width of the DE peak, for two values of the azimuthal angle φ in Fig. 9. For $\varphi = 0$, \vec{Q}_{\parallel} is perpendicular to the magnetization, and $\varphi = 0.3\pi$ corresponds to $\theta = 0.7\pi$ in Fig. 1. Again ω_0 and ω_s are the incident and scattered frequencies.

θ_I	Width for $\varphi = 0$ units of μH_0	Width for $\varphi = 0.3\pi$ units of μH_0
0.1π	0.021	0.034
0.25π	0.037	0.115
0.4π	0.059	0.202

In Sec. III we saw that width of the DE peak was determined by two factors: the transverse-spin-relaxation time, and the exchange-controlled loss of energy from surface spin waves to bulk spin waves. If the relaxation time τ is long enough, as the angle of incidence θ_I is increased one should be able to observe radiative broadening of the DE peak in the light-scattering spectrum. This broadening is a consequence of Q_{\parallel} increasing as θ_I increases since $|Q_{\parallel}| = 2\omega_0 \sin\theta_I/c$. As Q_{\parallel} increases, $DQ_{\parallel}^2/\mu H$ also increases and the exchange contribution to the width of the DE peak becomes larger as seen in Fig. 7 of Sec. III. We present our results for the width, of the DE peak in the light-scattering spectrum of Fe as a function of θ_I in Table II. In producing this table we have taken $1/\mu H \tau = 0.01$, a value quite reasonable for a well-prepared sample. We note that the broadening should be observable for propagation perpendicular to the magnetic field, but that it is larger for angles close to the critical angle; for $\varphi = 0.3\pi$ the width increases by about a factor of 7 in changing θ_I from 0.1π to 0.4π . This result is to be expected since, as we saw in Sec. III, the width of the DE peak in the spectral density increases as we approach the critical angle.

In Fig. 12 we display our results for the light-scattering spectrum near the critical angle. In Fig. 12(a) we examine the spectrum for propagation with $\varphi = 0.7\pi$. On the anti-Stokes side we see both the bulk and surface peaks and on the Stokes side just the bulk peak. As we move closer to the critical angle of $\varphi_c = 0.601\pi$ we see in Fig. 12(b) that the bulk and surface peak occur at the same frequency. Just past the critical angle at $\varphi = 0.6\pi$ we see in Fig. 12(c) that the spectrum on the anti-Stokes side has lost most of its sharp surface-spin-wave peak and the anti-Stokes side begins to look like the Stokes side. It will be intriguing to see experimental spectra with \vec{Q}_{\parallel} swung away from normal to the magnetization, to explore the DE wave near the critical angle.

In their paper, Wettling and Sandercock compare the position they find for the Damon-Eshbach and the peak in the asymmetric bulk-wave portion of

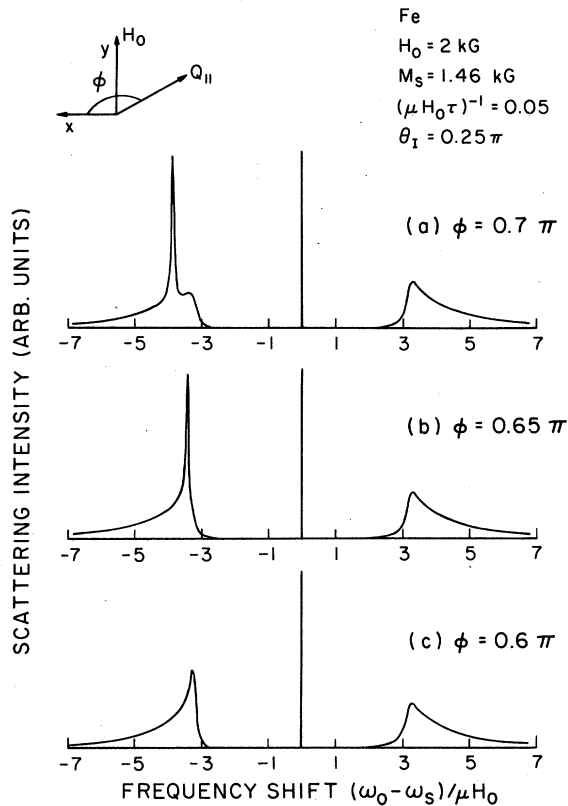


FIG. 12. Light-scattering spectra from Fe for angles of propagation near the critical angle, for the parameters used here $\varphi_c = 0.601\pi$. Thus in (c) we are looking just outside the region where surface spin waves propagate.

the spectrum with values calculated from the formulas which ignore the influence of exchange. They find the peak in the spectrum is quite close to $\mu(HB)^{1/2}$, with B calculated from the bulk magnetization of Fe. The DE wave appears to be lower than predicted from Eq. (3.1), and to account for this, they argue that the surface wave samples a region where the magnetization is lower than the bulk magnetization by possibly 15%. We believe that the incoming light samples thermal fluctuations only in the skin depth, and these exist in a region with a uniquely characterized (possibly spatially nonuniform) magnetization profile, i.e., the surface and bulk waves seen by the light see the same magnetization; other effects such as pinning may shift the surface wave relative to the bulk, however.

In our calculations of the Fe spectra, as remarked above, we find an exchange shift of the bulk spin wave that is appreciable, and substantially larger than the surface-wave shift. By choosing a *single* value of M_s some 15% lower than bulk Fe, we lower the frequency of the DE wave, but the upward exchange shift of the bulk wave

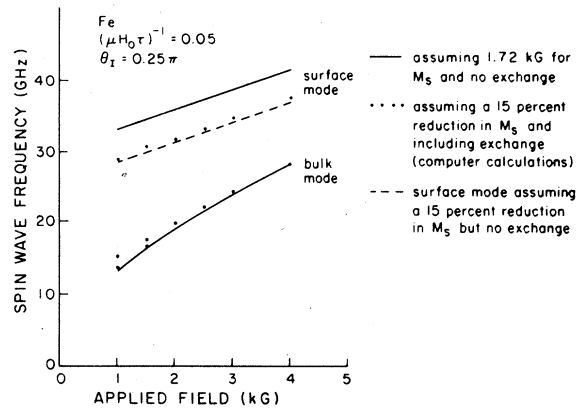


FIG. 13. Spin-wave frequency as a function of applied magnetic field.

comes close to canceling the downshift from the lowered magnetization. Our calculations are summarized in Fig. 13. The two solid lines show the bulk- and surface-mode positions as a function of magnetic field from the relevant formulas which ignore exchange. The dashed curve shows the DE mode calculated with no exchange, and a 15% reduction in M_s . Finally, the dots show the positions of both the surface- and bulk-spin-wave features in our calculated spectra with the full effect of exchange, and also a 15% reduction in M_s . For the bulk wave the dots lie very close to the solid line, and for the surface wave very close to the dashed line. Thus, a *single* value of M_s accounts for the position of *both* peaks. We have used $\gamma = (\mu H \tau)^{-1} = 0.05$, and the bulk-wave peak position is affected somewhat by the choice of γ , so the value of M_s we assign to the surface region is somewhat uncertain, though not greatly different than 15% below the bulk value.

In EuO, *both* the bulk-spin-wave peak and the DE peak lie below the values expected predicted from the bulk magnetization. The upward exchange shift is missing from the bulk wave, for reasons discussed above. We have not attempted a fit to this data.

There are tantalizing features of the data on both materials that prove most intriguing. If the reduced values of M_s are of intrinsic origin, further study of these spectra may provide fundamental new information about magnetism at surfaces. It is also striking that Grünberg and Metawe find a very strong temperature dependence for the frequency of the DE wave. This may have its origin in the magnetic surface reconstruction conjectured to occur on surfaces of Eu chalcogenides,^{4,5} but any conclusions at this time seem premature. Certainly detailed data on the temperature variation of the DE wave, particularly at lower temperatures, will be of great importance.

ACKNOWLEDGMENTS

We wish to thank Dr. J. Sandercock for a most stimulating discussion, and for a copy of his paper

with Wettling in advance of publication. This research was supported by U. S. Army Research Office, Durham, under ARO No. DAA 29-77-G-0101.

- ¹See, D. L. Mills and A. A. Maradudin, *J. Phys. Chem. Solids* **28**, 1855 (1967); D. L. Mills, *Phys. Rev. B* **1**, 264 (1970); D. L. Mills, *Comments Solid State Phys.* **IV**, **28**, 95 (1972); and the more recent very complete numerical analysis by K. Binder and P. C. Hohenberg [*Phys. Rev. B* **9**, 2194 (1974)].
- ²W. Saslow and D. L. Mills, *Phys. Rev.* **171**, 488 (1968).
- ³See D. L. Mills, *Phys. Rev. Lett.* **20**, 18 (1968); and also F. Keffer and H. C. Chow, *ibid.* **31**, 1061 (1973).
- ⁴S. E. Trullinger and D. L. Mills, *Solid State Commun.* **12**, 819 (1973); C. Demangeat and D. L. Mills, *Phys. Rev. B* **14**, 4997 (1976); C. Demangeat, D. L. Mills, and S. E. Trullinger, *ibid.* **16**, 52 (1977); D. Castiel, *Surf. Sci.* **60**, 24 (1976).
- ⁵C. Demangeat and D. L. Mills, *Solid State Commun.* **20**, 535 (1976); *Phys. Rev. B* **16**, 2321 (1977).
- ⁶P. K. Schwob, M. Tachiki, and G. E. Everett, *Phys. Rev. B* **10**, 165 (1974).
- ⁷J. T. Yu, R. A. Turk, and P. E. Wigen, *Phys. Rev. B* **11**, 420 (1975).
- ⁸P. Grünberg and F. Metawe, *Phys. Rev. Lett.* **39**, 1561 (1977).
- ⁹W. Wettling and J. Sandercock, *Am. Phys. Soc.* **23**, 388 (1978); and W. Wettling and J. Sandercock (unpublished).
- ¹⁰I. Hirada, O. Nagai, and T. Nagamiya, *Phys. Rev. B* **16**, 4882 (1977); T. Stakelon, *J. Appl. Phys.* **49**, 1592 (1978).
- ¹¹R. Q. Scott and D. L. Mills, *Phys. Rev. B* **15**, 3545 (1977); R. E. Camley and R. Q. Scott, *Phys. Rev. B* (unpublished).
- ¹²The films may have thicknesses that range from 200 or 300 Å (see Ref. 6) to a 1 μm (see Ref. 7).
- ¹³See the material in C. Kittel, *Quantum Theory of Solids* (Wiley, New York, 1963), Chap. 4.
- ¹⁴Wolfram and DeWames have analyzed the influence of exchange on the width of the Damon-Eshbach surface spin wave, for one propagation direction and in the limit where the influence of exchange is small. See T. Wolfram and R. E. DeWames, *Phys. Rev. B* **1**, 4358 (1970). These authors and their colleagues also completed experimental studies of modes in YIG films, under conditions where the role of exchange coupling is important. These data and their related theoretical work is summarized in T. Wolfram and R. E. DeWames, *Prog. Surf. Sci.* **2**, 233 (1972).
- ¹⁵D. L. Mills, Y. J. Chen, and E. Burstein, *Phys. Rev. B* **13**, 4419 (1976); and K. R. Subbaswamy and D. L. Mills (unpublished).
- ¹⁶J. S. Nkoma and R. Loudon, *J. Phys. C* **8**, 1950 (1975); J. S. Nkoma, *ibid.* **8**, 3919 (1975).
- ¹⁷R. Loudon, *Phys. Rev. Lett.* **40**, 581 (1978); K. R. Subbaswamy and A. A. Maradudin (unpublished); N. Rowell and G. Stegeman (unpublished).
- ¹⁸A. A. Maradudin and D. L. Mills, *Ann. Phys. (N.Y.)* **100**, 262 (1976).
- ¹⁹R. F. Wallis, A. A. Maradudin, and L. Dobrzynski, *Phys. Rev. B* **15**, 5681 (1977).
- ²⁰If $i=z$, we should relate the change in $\langle S_z(\vec{x}, t) \rangle$ to $\vec{h}(\vec{x}, t)$. Here we are exclusively concerned with the spin-wave regime, so we shall examine only the transverse response ($i=x$ or y).
- ²¹C. Kittel, *Phys. Rev.* **110**, 1295 (1968).
- ²²In magnetically ordered insulators, externally applied fields typically have strengths small compared to the internal exchange fields. Thus, if a low-frequency magnetic field is applied in a direction noncollinear with the magnetization, the dielectric tensor is altered not by the field itself, but rather the dominant contribution comes from the modulation of the exchange fields which result from the reorientation of the magnetization. A brief review of Faraday rotation in materials of interest to the present study is given by J. F. Dillon [*J. Appl. Phys.* **39**, 922 (1968)]. See also the data on TbIG reported by R. W. Cooper *et al.* [*J. Appl. Phys.* **39**, 565 (1968)]. This data shows a weak-magnetic-field dependence of the Faraday rotation tensor, for fields larger than those required to saturate the magnetization.
- ²³A very clear discussion of the effect of a magnetic field on the dielectric tensor may be found in L. D. Landau and E. M. Lifshitz, *Electrodynamics of Continuous Media* (Pergamon, Oxford, 1960), p. 331.
- ²⁴W. Wettling, M. G. Cottam, and J. R. Sandercock, *J. Phys. C* **8**, 211 (1975).
- ²⁵In Ref. 15, the analogous quantities were written in terms of two complex wave vectors k_1 and k_2 , both chosen with $\text{Im}(k_1) < 0$ and $\text{Im}(k_2) < 0$. Note that $k_1^{(S)}$ has a positive imaginary part, while $k_1^{(S)}$ defined in Eq. (4.9) has the opposite sign to its counterpart in Ref. 15.
- ²⁶C. Herring and C. Kittel, *Phys. Rev.* **81**, 869 (1951).